Fall 2016

Analysis of hindfoot alignment for total ankle arthroplasties

Heidi Kirsten Johanna Bingenheimer
University of Iowa

ANALYSIS OF HINDFOOT ALIGNMENT FOR TOTAL ANKLE ARTHROPLASTIES

By

Heidi Kirsten Johanna Bingenheimer

A thesis submitted in partial fulfillment
of the requirements for the Master of Science
degree in Biomedical Engineering in the
Graduate College of
The University of Iowa

December 2016

Thesis Supervisor: Assistant Professor Jessica Goetz

Graduate College
The University of Iowa
Iowa City, Iowa

CERTIFICATE OF APPROVAL

_____

MASTER'S THESIS

_____

This is to certify that the Master's thesis of

Heidi Kirsten Johanna Bingenheimer

has been approved by the Examining Committee for
the thesis requirement for the Master of Science degree
in Biomedical Engineering at the December 2016 graduation.

Thesis Committee: _____
Jessica Goetz, Thesis Supervisor

_____
David Wilder

_____
Nicole Grosland

“The journey of a thousand miles begins with a single step.”

Lao-tzu
The Way of Lao-tzu

ACKNOWLEDGEMENTS

I would like to acknowledge and thank Dr. Jessica Goetz for all the time and effort spent with me over the last year. It has been a pleasure working with you and getting to know you. Thank you for believing in me, encouraging me, and pushing me. I also want to acknowledge the University of Iowa Hospitals and Clinics Orthopedics and Rehabilitation Division. Particularly I would like to thank Dr. Phinit Phisitkul, Dr. John Femino, and Dr. Bryan den Hartog. I also want to thank Dr. Donald Anderson and the entire Orthopedics Biomechanics Laboratory. You all have been an incredible support and I have been absolutely blessed to be a part of the team. Last, but certainly not least, I want to thank my Lord and Savior Jesus Christ, my family, and my friends. Thank you for the countless hours of phone calls, prayers, reassurance, and inspiration provided.

ABSTRACT

Total ankle arthroplasties (TAAs) are mechanical devices used to replace the articular surfaces of the ankle joint in order to relieve pain for patients with osteoarthritis. Since most osteoarthritis is post-traumatic, and due to the highly variable individual foot geometry, TAAs are rarely inserted into normal geometry. This leads to serious problems with stresses and contact pressures in TAA components. This study uses finite element (FE) modeling to determine how hindfoot alignment, or how far in varus or valgus the most distal part of the calcaneus is perpendicularly from the axis of the tibia, affects the stresses and contact pressures in the articulating surfaces of two different TAA models.

To investigate the effects of foot alignment on hardware stresses after TAA, FE models were generated. Models of the mobile bearing, three component Scandinavian Total Ankle Replacement (STAR) and the fixed bearing, two component Zimmer Trabecular Metal Total Ankle (Zimmer) were generated from laser scans of the hardware and virtually implanted into 3D models of the tibia and talus. Ligaments were modeled as linear springs to impart physiologically realistic flexibility in the model. The stance phase of a walking gait cycle was applied and stresses and contact pressures at the articulation between model components were recorded for various degrees of hindfoot alignment [1].

Data analyzed shows that both models have areas of high concentrations of stress and contact pressure. The Zimmer TAA seems to favor a valgus alignment due to the lower stresses and contact pressures in valgus alignments compared to varus. Though the STAR does not generally favor one alignment over the other, it does have significantly lower stresses and contact pressures than the Zimmer. These differences may be due to the geometric congruency of the STAR versus the anatomical articulation of the Zimmer.

PUBLIC ABSTRACT

Total ankle replacements are devices used to help treat patients with pain in their ankles associated with arthritis. These devices replace damaged bone and cartilage on the tibia and talus with metal and plastic implants. Unfortunately, abnormally directed loads through the ankle joint can cause problems, and the replacement may wear out faster or even break depending on the severity of these abnormal loads. Patients with flat feet or high arches are at high risk for developing these abnormal loading patterns in their ankle replacements.

To determine how foot alignment may affect a total ankle, computer models of two different ankle replacements (the STAR and the Zimmer) were created. Normal walking was modeled and the way these models were supported was varied to simulate different degrees of flat and high-arch feet. The mechanical behavior of the total ankle replacement was studied to determine the effects of foot alignment.

From these models, it was found that the total ankle replacements are more tolerant of a flat-foot alignment, and that models simulating high had much higher stresses and could have a higher occurrence of breaking. Knowledge about the effects of foot alignment on total ankle replacement is important in order for surgeons to know how best to correct an ankle during replacement surgery and give the patient a better chance of a positive outcome.

TABLE OF CONTENTS

LIST OF TABLES

LIST OF FIGURES

CHAPTER 1: INTRODUCTION

Over the past 40 years, Total Ankle Arthroplasties (TAAs) have been used in European countries to treat patients suffering from osteoarthritis (OA), rheumatoid arthritis, or degenerative disease of the ankle joint, [1, 2]. TAAs eventually migrated to the United States where they have been successfully implanted with increasing regularity in recent years [3]. However, systematic biomechanical studies of the effects of foot and ankle alignment on stresses and contact pressures in TAA are scarce.

In TAA, the ankle joint is replaced using a metallic tibial component, metallic talar component, and a polymer bearing. This replacement attempts to eliminate pain, retain motion, and prevent OA in adjacent joints. Prior to TAA, ankle arthrodesis was considered the gold standard for treating complications such as OA or degenerative disease [4]. In ankle arthrodesis, the tibia and talus are fused together to eliminate the joint causing the patient's pain. Even now, ankle arthrodesis is still the preferred treatment in younger patients who lead active lifestyles and wish to return to such a lifestyle post-surgery, while TAAs are typically reserved for the more elderly/low-demand patient populations. This is due to the fact that ankle arthrodesis has been proven to be more stable and supportive than a TAA in terms of higher activity levels because of the fusion of the talus and tibia [5]. Due to the TAA being less stable and supportive, many patients with the need to remain active choose to forgo a TAA and be guaranteed the support of an ankle arthrodesis.

Although arthrodesis is still the preferred treatment in younger patients, TAA developers have been consistently working on engineering the components of TAAs to reduce the amount of bone removed during implantation, match the articulating surfaces

appropriately, and improve the amount of mobility and stability in the tibiotalar joint in order to provide less pain and improved motion of the joint. Despite potentially significant improvements in hardware designs, surgeons must make sure the alignment of the TAA hardware within the ankle is correct in order to benefit from the design improvements. If the TAA is not positioned correctly in the joint, or if the joint is very abnormally loaded, the TAA could be subjected to significant edge loading, increased polyethylene bearing wear, and subluxation all of which could lead to early failure [6]. Abnormal loading of the joint could cause further complications if the alignment of the foot – considered the calcaneus, talus, and tibia – is too far in varus or valgus alignment, also known as high-arch foot and flat-foot, respectively.

The alignment of the hindfoot is thus important to understand and determine for each patient. A normal, healthy hindfoot is very slightly in varus. A hindfoot alignment too far in varus or valgus can have serious complications if a corrective surgery does not accompany a TAA placement. These complications could include increased risk of failure of the TAA, increased risk of a break or sprain, and increased risk of OA developing in adjacent joints. Additionally, it is yet unclear what alignment of the hindfoot gives the patient the best outcome for a TAA placement. An understanding of ankle anatomy must be had in order to determine how hindfoot alignment affects TAA placement.

Ankle Anatomy

The ankle joint is defined as the articulation between the tibia, talus, and calcaneus. The tibiotalar joint, where the distal tibia and talar dome articulate, is generally considered the "true ankle" whereas the articulation between the talus and the calcaneus is the subtalar joint. Tension from ligaments, compressive forces of the gait cycle, and bony congruence between tibia and talus help maintain the structure and motion of the ankle during gait. The tibial medial malleolus and the fibular lateral malleolus form the ankle mortise and provide attachment sites for ligaments as well as articular surfaces which prevent the ankle from rotating or moving mediolateral and axial directions. The most mechanically stabilizing soft tissue structures which support the ankle are the deltoid ligament, the collateral ligament, and the syndesmosis [7]. The deltoid ligament is actually a complex of several distinct ligamentous bands originating from the medial malleolus and connecting to the anterior talus, the posterior talus, and the calcaneus. These distinct bands of the deltoid ligament are named the anterior tibiotalar (ATTL), the posterior tibiotalar (PTTL), and the calcaneotibular ligaments (CTL). The ATTL and PTTL are also known as the superficial deltoid whereas the CTL is also known as the deep deltoid. The collateral ligament originates on the fibula and connects to both the talus and calcaneus. The collateral ligament is often split into the anterior talofibular (ATFL), the posterior talofibular (PTFL), and the calcaneofibular (CFL) ligaments. Another well-known structure is the syndesmosis which connects the tibia and fibula throughout the interosseous space. The syndesmosis holds the tibia and fibula together and is created by the anteroinferior tibiofibular (AITF), the posteroinferior tibiofibular (PITF) and the interosseous tibiofibular (ITFL) ligaments. These ligaments, as well as the

bony congruency, help stabilize the ankle joint by keeping the bones in the proper position and following the gait articulation path.

In cases where the ankle is deformed in varus or valgus, the bony congruence and the ligaments are important as these structures attempt to keep the motion of the joint during gait from deviating too far. Bone congruency in deformed ankles could lead to impingement during gait and cause significant pain to the patient. In addition, ligaments in deformed ankles undergo significantly more stress and can deteriorate, leading to further instability of the ankle. Another factor that could cause complications of the ankle is OA which could lead to irregular geometry.

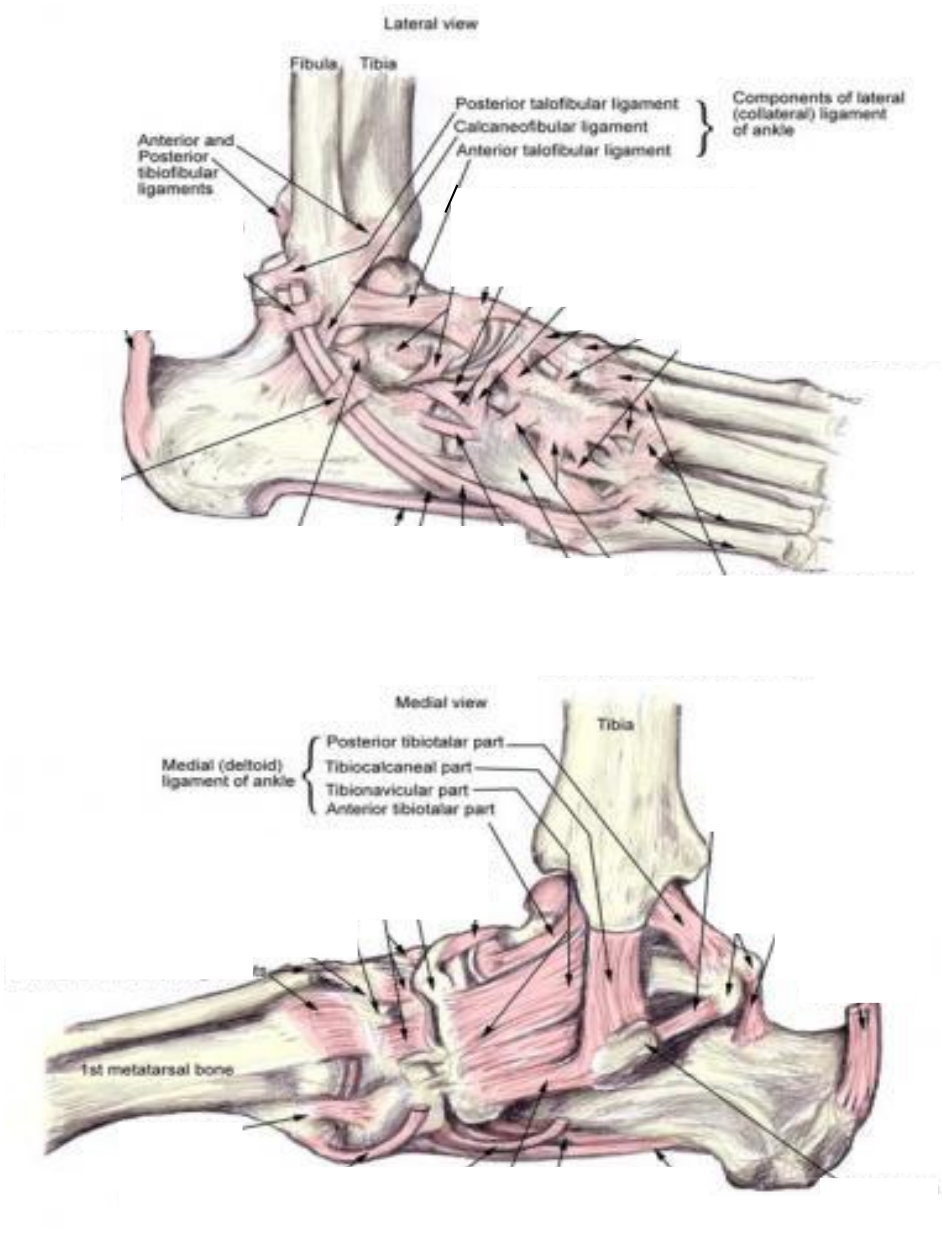

Figure 1. Ankle anatomy pointing out stabilizing ligaments (Hoagland 2015)

Osteoarthritis and the Ankle

Even though the tibiotalar joint has a small surface area over which to distribute force, the ankle can withstand five times the body weight of an average sized person. This is in contrast to the larger surface area of the hip joint, which is typically loaded to three times body weight [6]. Although the ankle is regularly subjected to large forces through years of walking, running, and jumping, osteoarthritis typically does not develop unless trauma to the ankle occurs. Such trauma can occur through fracture of the ankle or ankle sprains. OA, the most common reason for a TAA operation, causes a patient pain due to loss of cartilage, bone spurs, sclerosis, or cysts. These factors lead to pain, limited mobility, wearing away of the surface of the bone structure due to bone-on-bone contact, or even necrosis of the bones [8, 9]. Due to the wearing of the cartilage and the potential of damage to the bone, the extent of OA in an ankle may determine if a TAA can be performed. If the bone structure has is too weak or the talus has disintegrated, surgeons may chose to fuse the bone. Additionally, if the bone will likely not grow, an arthrodesis may be chosen since a failed arthrodesis is easier to repair than a TAA. The aim of TAAs is to reduce pain of OA and to retain motion so as to prevent further complications from OA at adjacent joints.

Arthrodesis

Introduced in 1879, ankle arthrodesis, or ankle fusion, is still considered the gold standard for treating patients with ankle OA[10]. Ankle arthrodesis may be performed using either external fixation, or open reduction internal fixation (ORIF). During both procedures, any remaining joint cartilage is removed and a bone graft may be placed into the joint to aid in fusion of the bones. In the external fixation method, an Ilizarov fixator, a metal structure containing holes for the screws, is used to guide k-wires, screws, and rods percutaneously into the bones [10]. The k-wires, screws, and rods pull the bones into contact and the compression helps encourage the fusion of the joint. When fusing with ORIF, the plates and screws rigidly connect the tibia to the talus [10]. Ankle fusion may additionally involve the calcaneus if the patient is experiencing subtalar OA [11, 12]. An alternative method of arthrodesis used in cases of multiple joint fusion is an intramedullary nail placed up through the bottom of the calcaneus to simultaneously fuse the tibiotalar and the subtalar joints. Throughout surgery, fluoroscopic images are obtained to ensure a proper alignment of the ankle with surgeons approximating the flexion angle, ensuring a slight varus alignment, and help the patient have the greatest chance of having a stable ankle.

An arthrodesis performed using any of these three techniques is completely stable leading to long-term successful clinical results. Consequently, younger patients with ankle OA tend to have arthrodesis as it is more robust under higher loads and usage under which the TAA may fail. Many studies have reported that patients, especially younger patients, have returned to normal levels of daily activity and have even returned to their

active lifestyles including running, biking, hiking, and even rock-climbing after arthrodesis [5, 10, 13, 14].

Total Ankle Arthroplasties

Figure 2. Models commonly used for Total Ankle Arthroplasty surgery. (From far left, STAR, Zimmer, and Salto Talaris)

TAAs have become more prevalent in the U.S in the past several years to treat patients with OA, especially in lower demand patients or those in which it is desirable to retain some tibiotalar motion. One of the main reasons TAAs are growing in popularity is studies in which gait has been analyzed post-surgery. Flavin et al. compared patients who received ankle arthrodesis to patients with TAAs and found TAA patients demonstrated a faster walking velocity due to increased stride length and cadence, as well as more normalized walking patterns [5]. TAA patients also had better dorsiflexion than arthrodesis patients and produced a ground reaction force similar to patients with normal ankles [5]. This study makes intuitive sense, as ankle arthrodesis is a joint fusion, making

the ankle joint a rigid structure and causing the patient to develop a new gait pattern. With a TAA, the patient has joint motion more similar to normal.

TAAs were introduced in Europe in the 1970s using implant designs with a highly constrained hinge motion, surgical implantation which required significant amounts of bone resection, and implant fixation using bone cement [2]. Due to the constraints of these earlier TAAs, many had high wear patterns which caused problems in the tibiotalar joint and adjacent articulations, and eventually early implant failure. Newer implant designs have evolved into less-constrained articulating components, the implantation of which requires less bone resection. Newer designs also have porous metal backing to promote bony ingrowth for fixation of the components. Several different types of TAAs have been approved by the FDA including fixed bearing and mobile bearing replacements as well as multi-pieced components or simple two component TAAs. This study explores two different types of TAAs: the mobile bearing, three component Scandinavian Total Ankle Replacement (STAR), and the fixed bearing, two component Zimmer Trabecular Metal Total Ankle Replacement (Zimmer). These two models were chosen due to the differences in each of the models components as well as the geometric articulation of the STAR model versus the anatomic articulation of the Zimmer model.

Scandinavian Total Ankle Replacement (STAR)

Figure 3. STAR Total Ankle Arthroplasty component structure

The STAR is a three-component, mobile-bearing TAA. Originally, the STAR was designed as a highly constrained two-component implant [2]. This design was caused complications such as severe edge loading and early failure of the polymer due to the ankle only being allowed to rotate in the sagittal plane. Additionally, the fixed polymer bearing, large amount of bone resection, and the added need for bone cement led to similar complications. The STAR was redesigned in 1986 to a mobile bearing three-component structure (Figure 3) which freed the joint to have more mobility and rotation [2].

The three components are the metallic tibial component, the metallic talar component, and the polymer spacer. Both the tibial and talar components are made from cobalt chromium while the polymer spacer is made of ultra-high molecular weight polyethylene. The tibial component has two cylindrical bars on the proximal side of a flat trapezoidal bearing surface. These cylindrical bars and the proximal surface of the tibial implant are covered with a porous metal coating to promote bone ingrowth. The distal

surface of the tibial component is polished and smooth. The talar component has fins on the medial and lateral sides of the component as well as a central keel to stabilize the component on the talar dome. As with the tibial component, the underside of the distal talar component also has porous metal coating to promote bone ingrowth [2]. The proximal talar component has a smooth cylindrical top which interfaces with the polyethelene spacer. The interfaces between the tibial and talar components and the polyethylene insert, are smooth with minimal friction (μ=.15) to allow for relatively free movement of the implant [15]. The talar component has a central rail on the bearing surface that interfaces with the polyethylene insert prevent the polymer bearing from moving medially or laterally and also prevents the component from internally or externally rotating. Thus, the polyethylene spacer can only rotate around the axis of the talar dome in the sagittal plane.

The tibial component of the STAR is inserted after the tibia is resected 5 mm proximal to the joint line. For the placement of the talar component, the proximal surface of the talar dome, as well as the medial and lateral gutters are resected to accommodate the fins of the talar component. Additionally, a fin of bone is removed from the center of the talar dome to allow the keel structure of the talar component to be placed. To implant the STAR, surgeons use an anterior approach.

Unfortunately there are aspects of the STAR design that cause concern for surgeons and surgical outcomes. First, the large amount of bone resected from the tibia and especially from the talus could disrupt the blood supply to the remaining bone, which in turn can cause avascular necrosis. If necrosis of the underlying bone occurs, the TAA could become loose and cause even more damage to the bone and surrounding soft tissue

structures. Additionally, retraction of the nerves and soft tissues overlying the joint during TAA surgery may disrupt the innervation of the great toe [16]. Another concern about the STAR is the rail interface between the polyethylene bearing and the talar component. Although the proximal side is free to rotate, the rail keeps the polymer bearing from rotating or translating in any direction except for rotation in a sagittal plane [2]. This could cause excessive stress, pressure, and wear on the polyethylene leading to a weakening of the bearing, premature failure, and the potential for detached polymer particles to irritate the joint. Due to the mobile bearing and three component structure, the STAR also relies on the tension of the ligaments to keep the polymer bearing from sliding out. If the ligaments do not provide adequate tension, as could occur if the patient has weakened ligaments or if additional bone resection was required, a thicker polymer component must be placed to increase the ligament tension sufficiently to hold the TAA components in place.

Zimmer Total Ankle Replacement

Figure 4. Zimmer Total Ankle Arthroplasty component structure

The Zimmer TAA is a two component, fixed bearing TAA that is thin and curved to reduce the amount of bone resected from the tibia and talus. The curvature of the talar

component better matches the curvature of the talar dome in multiple planes which provides motion similar to a normal, healthy joint [17].

The tibial component consists of a proximal cobalt chromium piece, which has two mediolateral rails (as opposed to the anterior-posterior rails of the STAR) and a porous coating to promote bone ingrowth. The polymer bearing rigidly snaps into the distal aspect of this tibial component, making it a single piece. The polymer bearing also has a bicondylar articular geometry which, due to the components being fixed in the bones, causes the tibia to externally or internally rotate during flexion and extension occurring in the sagittal plane [18]. This combined movement allows the components to provide a more natural movement of the joint during an individual gait cycle. The talar component also has a bicondylar geometry to match the polymer bearing. The talar component is thin compared to other TAAs, and attempts to mimic the curvature of the native talar dome [18]. This component also has the same porous coating and rails as the tibial component for fixation through bony ingrowth.

Unlike other TAA systems, surgeons use a lateral approach for the placement of the Zimmer TAA. This means that the surgeons must cut the fibula to reach the tibiotalar joint and then repair the fibula after TAA implantation. This approach allows the surgeons to burr out the bone in a curve similar to the ankle curvature and minimizes the disruption of the blood supply relative to other TAA models due to the semi-freehand aspect of the burring of the bone. Since the components have general curvatures similar to the healthy bone, the lateral approach allows for less bone to be removed [19]. The minimal resection of the bone in the tibiotalar joint helps prevent the loss of blood supply to the joint and decreases the chances of avascular necrosis of the remaining bone.

Although this design decreases the amount of bone resected, the lateral approach may cause other problems such as malunion of the fibula and increased disruption of innervation. The resection of the bone by burring, as described above, is more or less free-handed as the surgeon connects guidance holes placed by the surgical instrumentation accompanying the implant. Additionally, due to the lateral approach, the fibula is cut, rotated out of the way of the joint, and then plated back together post-TAA insertion [17]. This could cause nerves to be displaced and irritated or complete loss of sensation as well as blood supply cut off to the fibula.

Hindfoot Alignment View

According Saltzman in 1995, the Hindfoot Alignment View is the only radiographic view which shows the hindfoot position in relation to the tibia [6, 20]. One way to get a better view on how the TAA replacement should be inserted in the ankle is this Hindfoot Alignment View. Hindfoot alignment view (HAV) radiographic imaging for diagnostic purposes helps surgeons view whether a patient's foot is in varus or valgus alignment [6]. For most diagnoses of ankle OA, patients have radiographs acquired from multiple angles/positions. HAV is especially important in TAA placement due to the determination of the degree of flatfoot or high-arch deformity as well as how the extent of ankle deformity. If there is a significant malalignment which is not corrected, TAA placement can lead to further damage to the ankle joint of the patient by causing edge loading, early failure of the TAA, or avascular necrosis. Therefore, correct placement of the TAA is key for the outcome of the surgery. The angle of placement of the TAA in the ankle could cause loading problems leading to wear and early failure [21].

Additionally, surgeons must determine the proper placement of TAA for each patient based on the varus or valgus alignment of the patient's ankle. For this reason, HAV is used to visualize the deformity of the foot and determine how far in varus or valgus the foot is malaligned.

The HAV is taken at a 20-degree angle to the horizontal axis of the foot, generally represented by the floor, and at a distance of 40 inches from back of the weight-bearing ankle. The foot is placed so that the beam of the X-ray is parallel to the medial border of the ankle joint [20]. This image shows the posterior calcaneus, talus, tibia, and fibula. Hindfoot alignment is then determined as the perpendicular distance from the tibial axis to the most distal part of the calcaneus.

The average Hindfoot Alignment View Distance of a normal, healthy ankle is approximately 2.5mm in varus and the range for "normal" hindfoot alignment is approximately 8 mm in varus to 5 mm in valgus [22]. More extreme deformities will likely need to have hindfoot corrective surgery in addition to TAA. The extent to which a hindfoot can be in varus or valgus before a corrective surgery must occur or what the effect of such deformity, if not corrected, would be on a TAA is yet to be determined. It is known, however, that proper hindfoot alignment is required to decrease the chances of implant edge loading, polyethylene bearing wear, and subluxation, which is important to prevent early failure of the TAA.

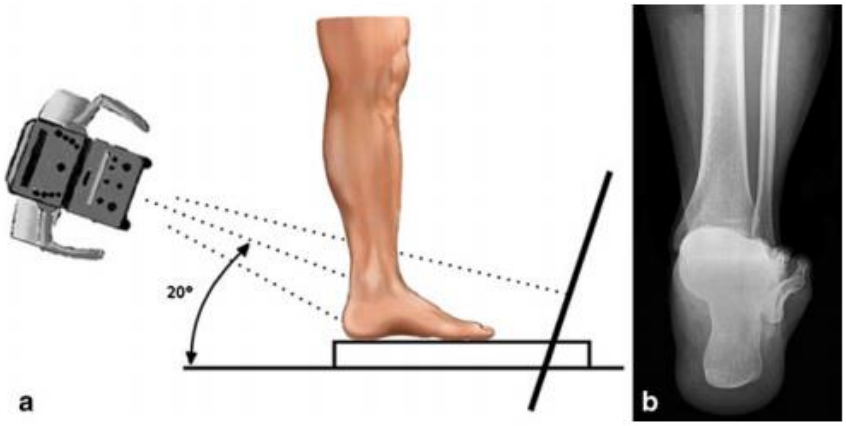

Figure 5. Hindfoot Alignment View. The camera is inclined at a 20 degree angle to the horizontal floor and fluoroscopy is produced along the tibial axis

Finite Element Analysis

Finite Element Analysis (FEA) is a computational modeling technique that has been used in multiple fields of research such as construction, aerospace, and orthopedics to determine force and stress distributions, displacements, and failure modes in irregularly shaped objects. Previous FEA studies of TAAs have shown that the majority of contact pressures in TAAs remain between 10-30 MPa with the average peak contact pressure being about 50 MPa [15, 23]. Some of these studies use models which were created to mimic FDA approved TAAs, while other studies have investigated models that are not currently implanted [15]. However, few studies have been performed which use the geometries of the actual replacement components as well as surrounding anatomy (talus, tibia, fibula and ligaments). Thus these studies use approximations and do not have models similar to local anatomy.

Purpose

In this study, FEA was used to determine the contact stresses in the components of the TAA with varying amounts of hindfoot malalignment. Total ankle arthroplasties replace the native joint with mechanical components to alleviate pain for patients with OA while retaining motion of the joint. Unfortunately, underlying malalignment of the hindfoot could cause the TAA to be subjected to abnormal and/or high stresses and cause negative outcomes for the patient. This study focuses on simulating differing degrees of varus and valgus hindfoot alignment to determine the extent to which a hindfoot can be malaligned while maintaining stresses, contact pressures, and movements that do not deviate much from baseline.

CHAPTER 2: MATERIALS AND METHODS

Surface Generation

The first step to produce finite element models of TAA was to obtain 3D surface geometry of the TAA components. This geometry was obtained using the laser scanning setup shown below. A laptop running ScanStudio software (NextEngine Inc., Santa Monica, California) was connected to a 3D laser scanner and part rotator (NextEngine Inc., Santa Monica, California). Prior to laser scanning, each of the components was dusted with talcum powder to reduce the surface reflectivity, so that the surfaces could be more accurately detected by the laser scanner. Each TAA component was scanned at 30° intervals around the entire component. These twelve increments were automatically combined in the software based on common geometry to form a single surface of the TAA. Due to the method of acquisition by the laser scanner itself, all geometry in the field of view were scanned. Since the platform and holder of the component were often in the laser scan, parts that showed up on the laser scan which were not actually the component had to be removed. The sections that were removed from the surfaces contain the platform of the part rotator as well as the rubber arm which holds the component in position as can be seen below.

This process was repeated on each component while in varying component orientations (i.e. turned on its side or supported on one of the corners). Three scanning positions were required in order to visualize the full 3D geometry of the component with the laser.

The three scans from each 360 degree pass in the different component orientations were then exported as .stl files and imported into Geomagic software for alignment and surface refinement (3D Systems Inc., Rock Hill, South Carolina).

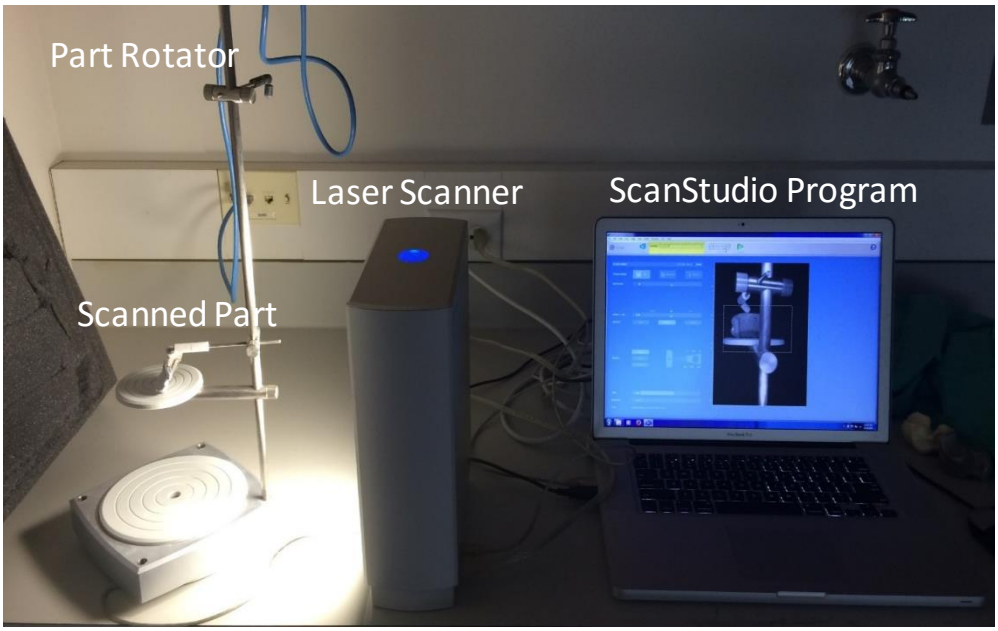

Figure 6. Laser Scanning Setup Showing the ScanStudio Program, Laser Scanner, and Part Rotator

There, the "best fit" function used the geometry of each scan to rotate each scans to be aligned correctly and then merged the scans to make a singular surface. Once the scans were aligned and merged, any remaining holes in the surface were filled. The component's surface was then smoothed to remove any spikes or triangles that did not appear to be part of the actual component piece. These components were then geometricized to simplify the later mesh generation while keeping the integrity of the geometry of the structures. This included projecting the surface to geometric planes and cylinders to smooth the porous metal backing of the components as well as fit the geometry to regular shapes.

Figure 7. Example of laser scanned object additionally showing the platform and holder components

STAR TAA Model

For the STAR model, the tibial component was simplified to have two cylindrical rails. This was performed by creating geometric cylinders from the scanned implant surface and projecting the scanned cylindrical surfaces onto those geometric cylinders. The top and bottom of the base of the tibial component were projected to parallel planes defined from the scanned geometry of the tibial component. The polymer component for the STAR model was projected to several intersecting planes using the "best fit" function in the Geomagic software. The best fit function enabled the scanned surface of the polymer to essentially be a template for the planes used to smooth and make the edges of the polymer more precise. The curved center of the polymer bearing where the polymer component interfaces with the talar component was projected to a geometric cylinder (excluding the groove to interface with the talar rail). The axis of this geometric cylinder was then referenced in order to create a cylinder with a slightly smaller diameter to geometricize the talar interface with the polymer bearing. This slightly smaller diameter was defined to allow the polymer component to interface over a larger surface area of the talar component and help seating of the components occur. Additionally, the underside of

the talar component, the inside of the medial and lateral fins, and the sides of the keel of the talar component were all projected to planes that were best fits of the scanned implant geometry. The geometry of the rail interface between the polymer component and the talar component was maintained as it was scanned. This geometry was maintained due to the important interface between the components as well as to ensure that more realistic stress and contact pressure values were obtained. Similarly, the exterior geometries of the medial fin, the lateral fin, as well as the curvature of the interior keel of the talar component were maintained from the scan.

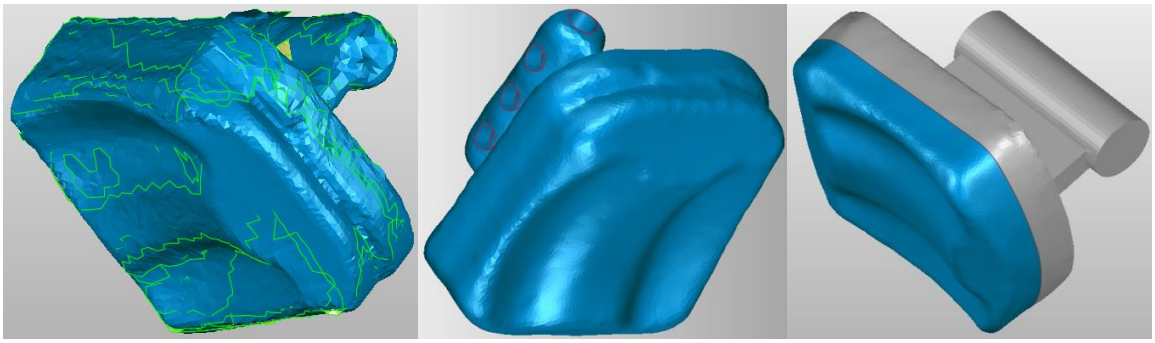

Figure 8. Example of filling holes, removing spikes, resurfacing, smoothing, and geometricizing of components. This TAA model is not used in this study.

Zimmer TAA Model

The geometricizing of the Zimmer components involved projecting the bottom of the talar component and the top of the tibial component to two different geometric cylinders. The two rails on both the talar and tibial components were projected to rectangular prisms. Due to the complex bearing surface geometry of the Zimmer TAA, the remaining surfaces were not geometricized and were left as scanned from the geometry of the component.

Bone Surface Creation

The surface models for the bones used in this study were obtained from MRI scans of a normal ankle that has previously been segmented using OsiriX software (Pixmeo, Geneva, Switzerland). These segmentations were saved as point clouds which were then loaded into the Geomagic software for surface generation, including hole filling and smoothing

These bony surfaces were modified to accommodate the TAA hardware according to a combination of each implant's surgical technique guide, TAA component surfaces, and verbal input from two foot and ankle orthopedic surgeons (University of Iowa Department of Orthopedics and Rehabilitation).

STAR Virtual Implantation

To accommodate the STAR TAA, the tibia was resected five millimeters proximal to the distal tibia surface. To digitally perform this resection, the surface of the distal tibia was projected to a plane 5 mm proximal to the joint that was representative of the cut which a surgeon would use upon tibial component placement. This step did not involve the medial malleolus. Next, the lateral surface of the medial malleolus was trimmed using a plane which intersected with the plane of the distal surface of the tibia and the trimmed surface was projected to the new plane in order to fit the tibial and talar components. However, care was taken to not resect too much from the medial malleolus as physiologically, the medial malleolus is one of the most fractured structures post-TAA placement. The amount of resection was reduced by angling the plane so the proximal part of the plane was more lateral. The medial malleolus is also critically important for

ankle stability after TAA as it is the origin of the deltoid ligaments which support the medial side of the ankle [24].

The talus was virtually resected using the planes created from geometricizing the interior of the component as well as the keel after the placement of the talar component occurred. The talar component was placed on the talus based on the surgical technique guide as well as visual assistance from foot and ankle surgeons. From this, the medial and lateral sides of the talus were trimmed accordingly to ensure the fins of the talar component did not impinge on the talus bone itself [16].

Zimmer Virtual Implantation

The tibia and talus had curved resections simulated for virtual implantation of the Zimmer TAA model that were based on the surgical technique guide [18]. The cuts for both these bones begin with a series of drill holes the surgeon places based on guiding tools in the distal part of the lateral tibia and the proximal part of the lateral talus. These holes are systematically placed for the fixation the cylindrical base of the tibial or talar component into the distal tibia and proximal talus, respectively. The holes are then connected using a burr in between the holes and create the curved cylinder. The rails for the tibia and talus are also created from drill holes using a surgical guide. For virtual implantation, the tibial and talar components were placed in the joint space, overlapping the bone surface, and the intersecting surface of the bone was cut to match the surface of the implant. The tibial component's resection was approximately five millimeters proximal in the bone and the talar resection was based on the placement of the tibial component to attempt to resect as little bone as possible. The surfaces of the tibia and

talus were then simplified by the cylinders which were used to create and simplify the tibial and talar components.

Mesh Generation

The .stl files for each component and bone surface were imported into TrueGrid (XYZ Scientific Applications Inc., Livermore, California) for mesh generation. TrueGrid uses block structures to produce a solid hexahedral mesh from a simple triangulated surface. Simple block structures are defined specifying numbers of elements and projected to basic geometric surfaces defined within the software or by .stl representations of the complex bone and TAA component surfaces. One key meshing technique used in this work was used repeatedly throughout meshing the TAA components and bones. In this technique, a block structure with an equivalent number of elements on the corners is created. From this structure, the corner blocks are deleted and "block boundaries" are created which make the remaining two edges of the deleted block combine to one interior block edge. The butterfly technique not only helped to create not only a better looking mesh, but was important to maintain the orthogonality of elements around the curves of each TAA component and bones. This simple, yet powerful technique is shown in Figure 10 while creating one of the cylindrical rails for the STAR model.

Many of the TAA components were subdivided into more simple geometric sections for meshing. For example, the STAR tibial component was separated into two cylinders and a flat base. These subdivided meshes were then equivalenced together to create the full component mesh. Prior to exporting the meshes from TrueGrid, the models were all re-oriented to be aligned to a common coordinate system with the x-axis directed

along the medial-lateral axis of the bones, defined as the axis aligning the tip of the lateral malleolus of the fibula to the tip of the medial malleolus of the tibia. The y-axis lies in the sagittal plane while the z-axis was directed along the tibial shaft.

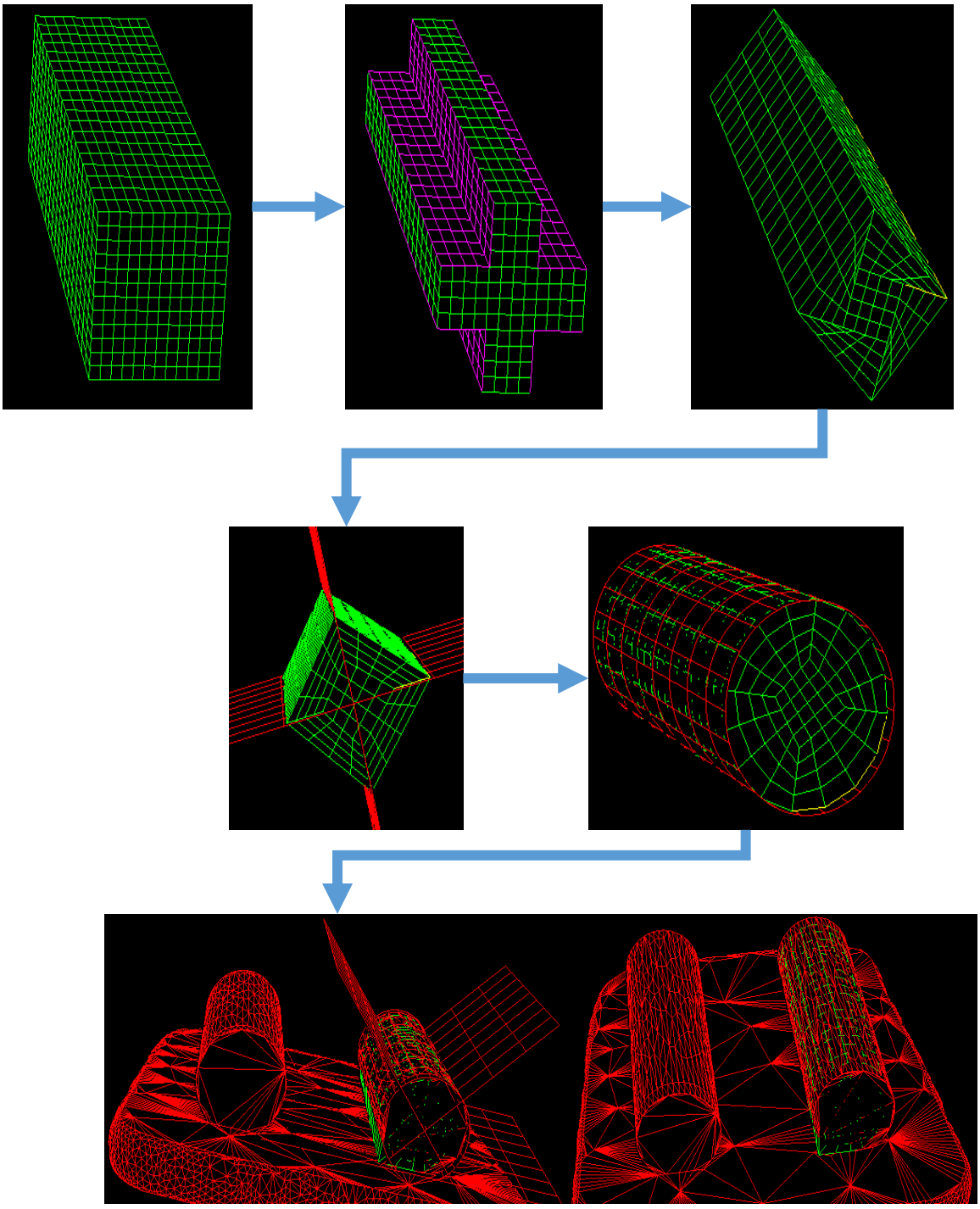

Figure 9. Example of butterfly technique often used in TrueGrid meshing starting with a 3x3 block structure created in TrueGrid (green), deleting the corners, applying block boundaries, and projecting to defined planes, geometric cylinders, and the .stl surface of the tibial component surface (red)

Gait Modeling, Stress, and Contact Pressure Generation

The meshes exported from TrueGrid for both the STAR and the Zimmer models – the talus, talar component, tibial component, polymer component, tibia and fibula – were then assembled in the ABAQUS input deck. Within the input deck, the material properties of each element were assigned, the contact interactions between model components defined, and the forces and the rotations were applied. Springs were also defined in the input deck to represent several of the important ligaments in the ankle joint. For this study, the material properties for each part of the models and bones are shown in Table 1 below.

Table 1. Mechanical Properties of Solid Components

	Cobalt Chromium Metal	Ultra-High Molecular Weight Polymer	Cortical Bone
Young's Modulus (E)	220000	500	12000
Poisson's Ratio (v)	0.25	0.4	0.3

To simulate the gait cycle, graphs of ankle forces and rotations created by Stauffer et al. were digitized. In his 1977 article, he described a 2D method to analyze the gait cycle in the sagittal plane and using specified angles for each phase of a gait cycle, charted the forces acting on the ankle joint using a force plate and simple trigonometry [1]. From these charts, thirteen data points were discretized from the graphs in equal increments spanning the stance phase of a single gait cycle [25]. These data points described the degrees of ankle flexion, as well as the compressive forces through the joint for each increment. The degrees of ankle flexion in the sagittal plane were converted to radians, and the magnitudes of the axial compressive forces were determined. Except for the hardware only models, assigned to the FE models using reference nodes tied to a rigid

body defined at the proximal-most region of the model. Gait loads were applied using a follower load option which applies the load perpendicular to the joint surface at each joint rotation. All models were run in ABAQUS.

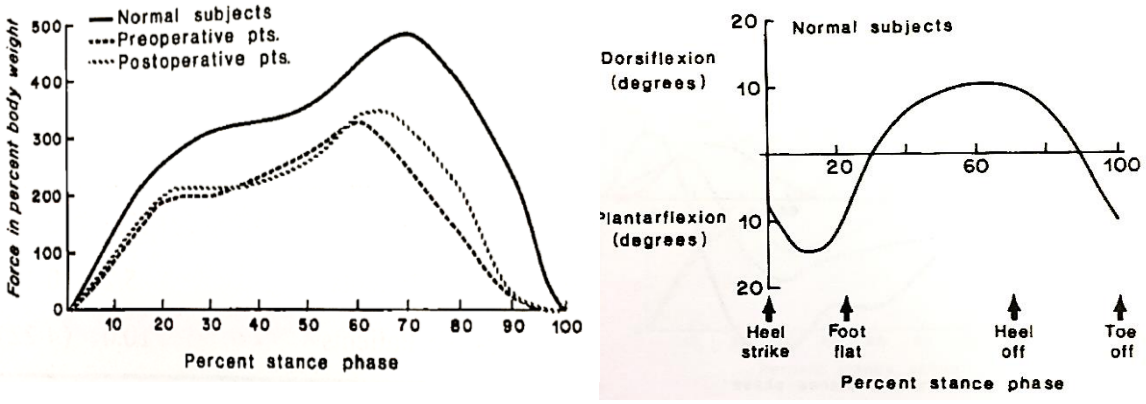

Figure 10. Force and rotation data showing the force and rotation in degrees for gait [4]

To build the complexity of the models and minimize the time taken to run the models, and for the purposes of needing to troubleshoot before increasing the complexity of the models, both the Zimmer and the STAR models started out with just the hardware components. In both hardware-only models, the entire bottom surface of the talar hardware component (where it would interface with the underlying bone) was held fixed in the x, y, and z directions by constraining all nodes on the surfaces. In order to prevent problems with initial contact associated with mesh discretization from allowing the models to run, each model began with a very small space between the components. Therefore, the initial step was to establish contact of the components by prescribing a downward displacement equal to the distance between the components. This displacement was applied to the tibial component via the reference node associated with the top of the tibial component. In the STAR model, the polymer bearing was constrained from moving in the mediolateral and the anterior-posterior directions in order to prevent

it from migrating out from between the metallic components before it was fully in contact with both the upper and lower bearing surfaces. After the first step to establish contact, the displacement boundary condition was replaced by a downward force, also applied to the same tibial reference node, which was equivalent to the -222.4 N vertical force at heel strike. In the next two steps, the vertical force was separated into a compressive axial force as well as a small anterior-posterior force and was applied along with the rotation associated with heel strike. After these initial 4 steps to establishing contact and position the model for heel strike, the boundary conditions on the polymer and tibial components were released to allow axial and coronal rotation. This allowed the model to more realistically simulate component motion during the subsequently applied thirteen incremental rotations and forces determined from the digitized graph to encompass the stance phase of gait. Table 2 below shows the rotations and forces for the tibial components. Due to difficulty in reaching convergence with the originally discretized 13 steps spanning the stance, an additional step was added between step 2 and 4 to help with the rotational change from a -0.07 radian posterior position to 0.014 radian anterior. Though the rotation was subdivided, the applied force was left the same for this added step.

Table 2. Rotations and compressive forces applied to the model to simulate gait cycle

Step	Gait Rotation (radians)	Tibia Compressive Force (N)
1	-0.061	-222.4
2	-0.07	-756.2
3	0	-756.2
4	0.014	-1512.4
5	0.056	-1734.8
6	0.086	-1823.8
7	0.096	-2250.8
8	0.11	-2535.5
9	0.131	-2829.1
10	0.155	-2197.4
11	0.16	-1378.9
12	0.105	-578.3
13	-0.035	-100
14	-0.096	-50

After the hardware-only models were running to completion, the talus bone was added. The steps to establish contact and were similar to the simple hardware model, however the talus was held in all directions via a reference node associated with the bottom of the talus. The interface between the talar component and the talus bone was equivalenced to be one structure and simulate attachment of the talar component to the talus with bony ingrowth. The talus was constrained in all directions via a reference node associated with the bottom of the talus, but located at the center of rotation for the components. The steps to establish contact between the components were identical to the simple hardware model and the gait cycle remained the same. This version showed that adding bone structure doesn't completely change the motion of the ankle replacement or the stress and contact patterns of the components

Next, the tibia bone was added. As described above for the talus, the elements between the tibial bone cuts and the tibial component were equivalence to simulate bony ingrowth fixation. The boundary conditions applied to the talus and talar component were identical to those described in the previous paragraph. The reference node for the tibia and tibial component was placed at the center of rotation for the sagittal rotation of the joint and associated with the top of the tibia. Other than a change in which elements the reference node was associated with, all boundary conditions, rotations, and applied forces remained the same as prescribed to the hardware-only and hardware plus talus models. The goal of this model set was to determine if addition of bones between the boundary conditions would alter the TAA component stresses.

In order to be able to change the hindfoot alignment, the next step was to add the fibula and ligaments. While there are no components of the TAA hardware implanted in the fibula, it was an important structure to include as it is the attachment site for many stabilizing ligaments and may impinge on the talus or TAA hardware in severely varus or valgus foot conditions. To make the model anatomical, the deltoid ligaments, the collateral ligaments, and the syndesmosis ligaments were added for the stabilization of the joint. These ligaments allow for rotational constraint of the ankle, without prescribing direct non-rotating boundary conditions.

In the initial steps to establish contact, the talus is held in place in the x, y, and z directions via a reference node associated with the bottom elements of the talus while a downward displacement is applied to the tibia and fibula at two different reference nodes associated with the top elements on each of the tibia and fibula surfaces. The tibia reference node was placed at the center of the sagittal rotation of the ankle joint and the

talar reference node was placed 10mm distal to the tibia reference node in the z axis. The initial seating steps are exactly the same as the previous models. However, at this point, the coronal and axial rotation constraints on the talus were released, allowing the talus to move in a more anatomic fashion that was governed by ligamentous support and implant geometry rather than fixed boundary conditions. The talus reference node remained fixed in the z-direction to prevent translation in the superior/inferior direction. After these steps to establish contact with less rigid boundary conditions, the fourteen loading steps simulating gait described earlier were applied. Because the fibula was present in these models and it bears a small fraction of the load during gait, the load values were split so 83% of the force occurring at heel strike was applied to the tibia while the other 17% was applied to the fibula [26]. In order to compare the structural stability the syndesmosis provides for the ankle and how this structural stability affects the stresses and contact pressures in the hardware components, three ligaments, representing the high, middle, and low syndesmosis areas, were applied. Models both with and without the syndesmosis ligaments were created for the Zimmer TAA. The STAR models were only run with the syndesmosis.

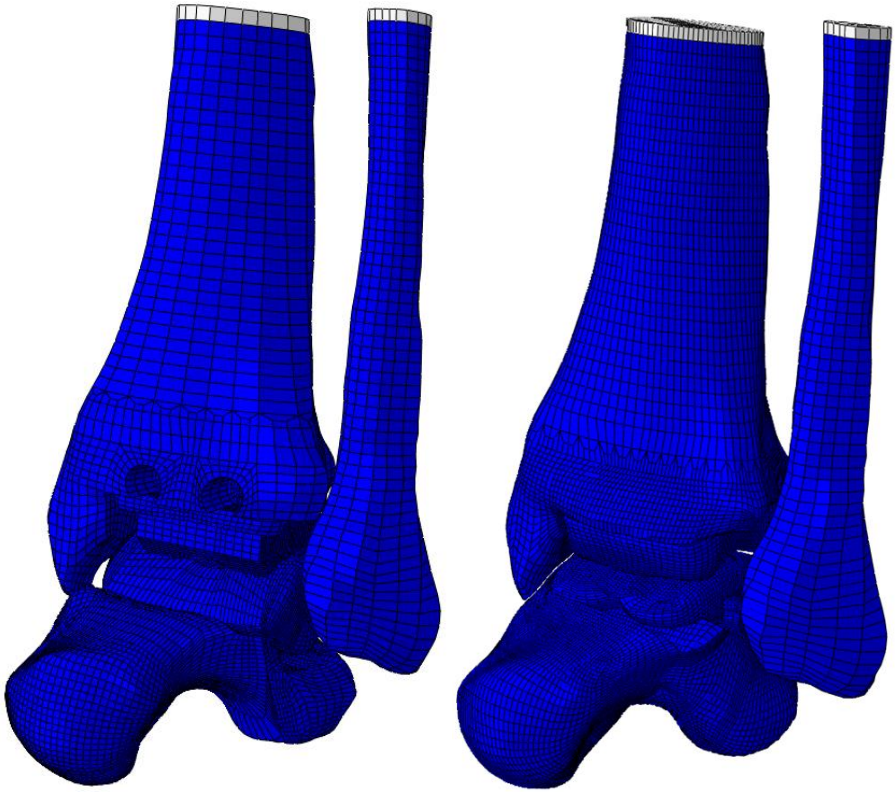

Figure 11. Abaqus Model for STAR TAA (left) and Zimmer TAA (right) (springs are difficult to see and were left out of the Figure)

After establishing all the relevant anatomy, hardware components, and model definitions, the hindfoot alignment was varied. Approximately 50% of the population has non-normal foot alignment which could increase or shift implant stresses and negatively affect survivorship of the implant within surrounding bones [3]. To simulate a change in hindfoot alignment, the talar reference node was moved medially or laterally to simulate hindfoot varus or valgus, respectfully. The "baseline" models had the talar reference node placed to simulate -2.5 mm of varus of the distal calcaneus and is representative of implanting a TAA into an ankle with average hindfoot alignment. Several models in 2.5 mm or 5 mm increments were created in varus or valgus from the baseline. Varus values are indicated by negative values, which are medial to the baseline conditions, and the

valgus values are positive, or toward the lateral side. Several are still considered to be in the range of "normal" hindfoot alignment and have been labeled as normal with A, B, and C being increasing deviation from the baseline model. Higher malalignments then are labeled as slight, moderate, and extreme in the increasing severity of the foot alignment. Simple trigonometry was used to determine the positions of the reference node for each of twelve hindfoot alignments for each model. The vertical distance from the center of rotation to the most distal part of the tibia and the perpendicular hindfoot alignment view distance were used as the two sides of a right triangle. Once the length of the hypotenuse was found, and since the talar reference node was located 10mm distal along the vertical distance from the center of rotation, this triangle was used as a similar triangle to find the medial or lateral distance the talar reference node should be moved to simulate the corresponding hindfoot alignment. These positions corresponded to a range of hindfoot valgus of 25mm to a hindfoot varus of -25mm. The twelve incremental changes in the hindfoot alignment is defined in Table 3 below. The maximum stresses at each step as well as the maximum contact pressures for the interface of the surfaces were extracted.

Table 3. Alignment Range Based on Hindfoot Alignment View Distance Measurements

Alignment	Values (mm)
Extreme Varus	-25
Moderate Varus	-20
Slight Varus	-15
Normal Varus B	-10
Normal Varus A	-5
Baseline	-2.5
Normal Valgus A	0
Normal Valgus B	5
Normal Valgus C	10
Slight Valgus	15
Moderate Valgus	20
Extreme Valgus	25

CHAPTER 3: RESULTS

The maximum von Mises stresses were extracted from each of the 12 hindfoot alignment models with both implants. The stress results were recorded from the peak stress at the completion of each step in just the hardware components. For the Zimmer model, maximum contact pressures between the polymer bearing and the metallic talar component were recorded for models both with and without the syndesmosis. For the STAR model, maximum contact pressures were extracted from the interface between the metal tibial component and the top of the polymer bearing as well as at the interface between the bottom of the polymer spacer and the top of the metallic talar component. In general, maximum stresses and contact pressures varied according with increases and decreases in the forces applied over the duration of the gait cycle.

The purpose of the including bones was to create a more realistic gait model and allow for movement of the ankle model similar to a healthy ankle. Because many of the degrees of rotation in the final models were not held, the talus was allowed to rotate which led to slight tilting of the talus both medially and laterally. This correlates to the rotation the talus is able to have against the calcaneus in a healthy ankle. The graphs, which record the stresses and contact pressures over the modeling steps of a single gait cycle, show the differences between the varus alignments and the valgus alignments. In general, the varus alignments caused higher stresses and contact pressures whereas the valgus alignments showed varying results for the two models.

Zimmer TAA

Models both with and without the syndesmosis were run for the Zimmer model in order to compare how the added flexibility of the syndesmosis would affect the stresses and the contact pressures in the TAA components. In general, the maximum von Mises stress and the maximum contact pressure were higher in the models with syndesmosis.

The maximum von Mises stresses occurred in the rails while the maximum contact stresses seemed to occur along the domes of the talar component. Due to the added change in rotation step, the large stress jump at the beginning of the data set occurs. There was no contact between the fibula and either the talus or the TAA component in any of the modeled hindfoot positions. However, high stresses in the ligaments occurred in the extreme models.

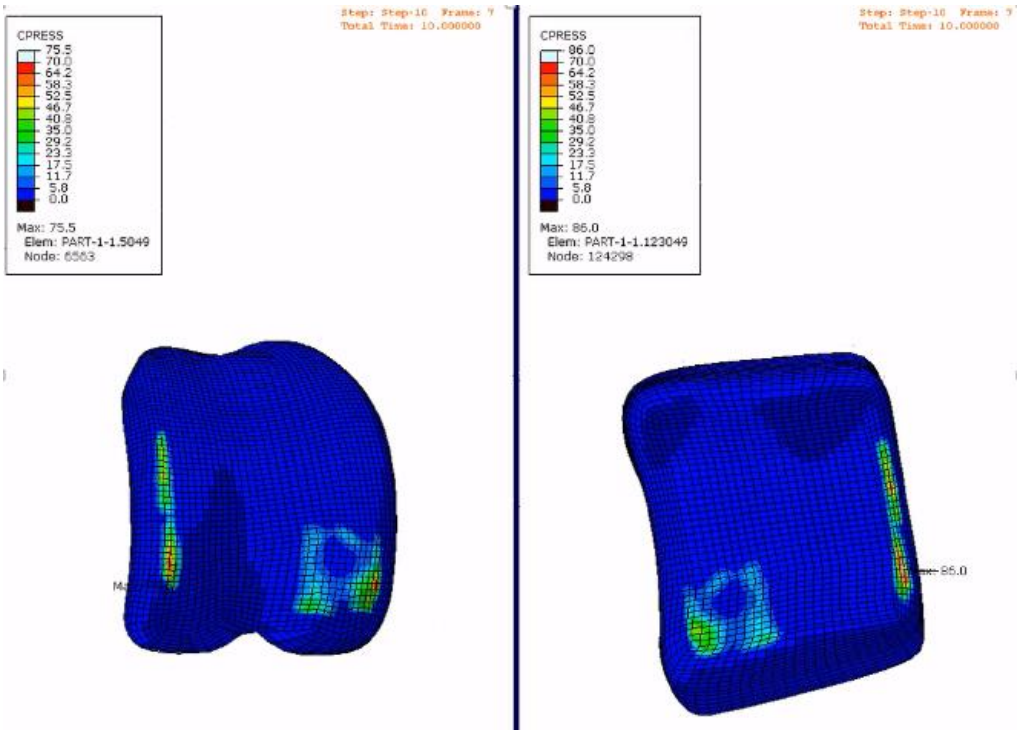

Figure 12. Zimmer Total Ankle contact presure between talar component (left) and tibial component (right)

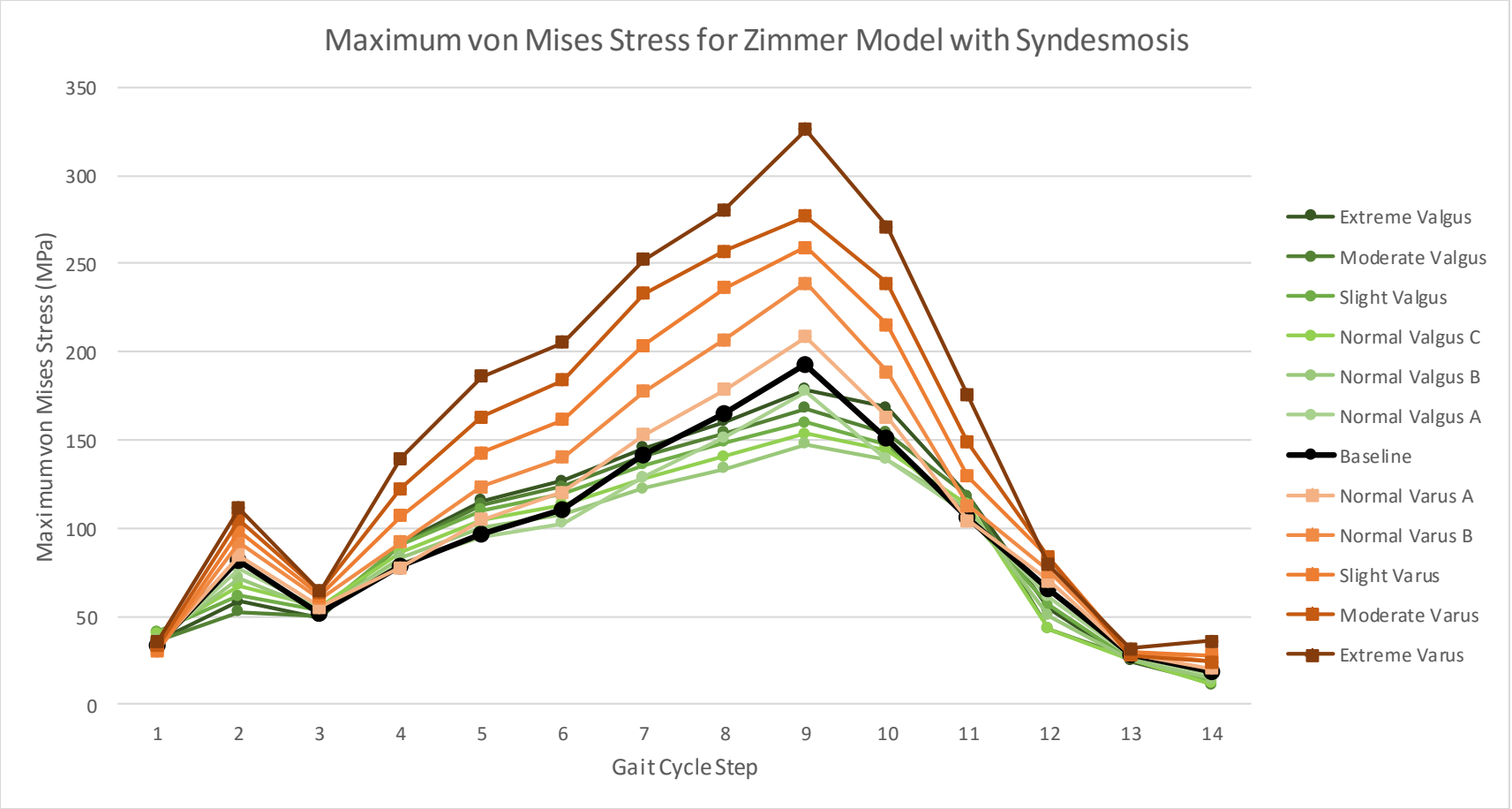

Figure 13. Maximum von Mises Stress for the End of Each Gait Cycle Step for the Zimmer TAA Model with Syndesmosis Ligaments

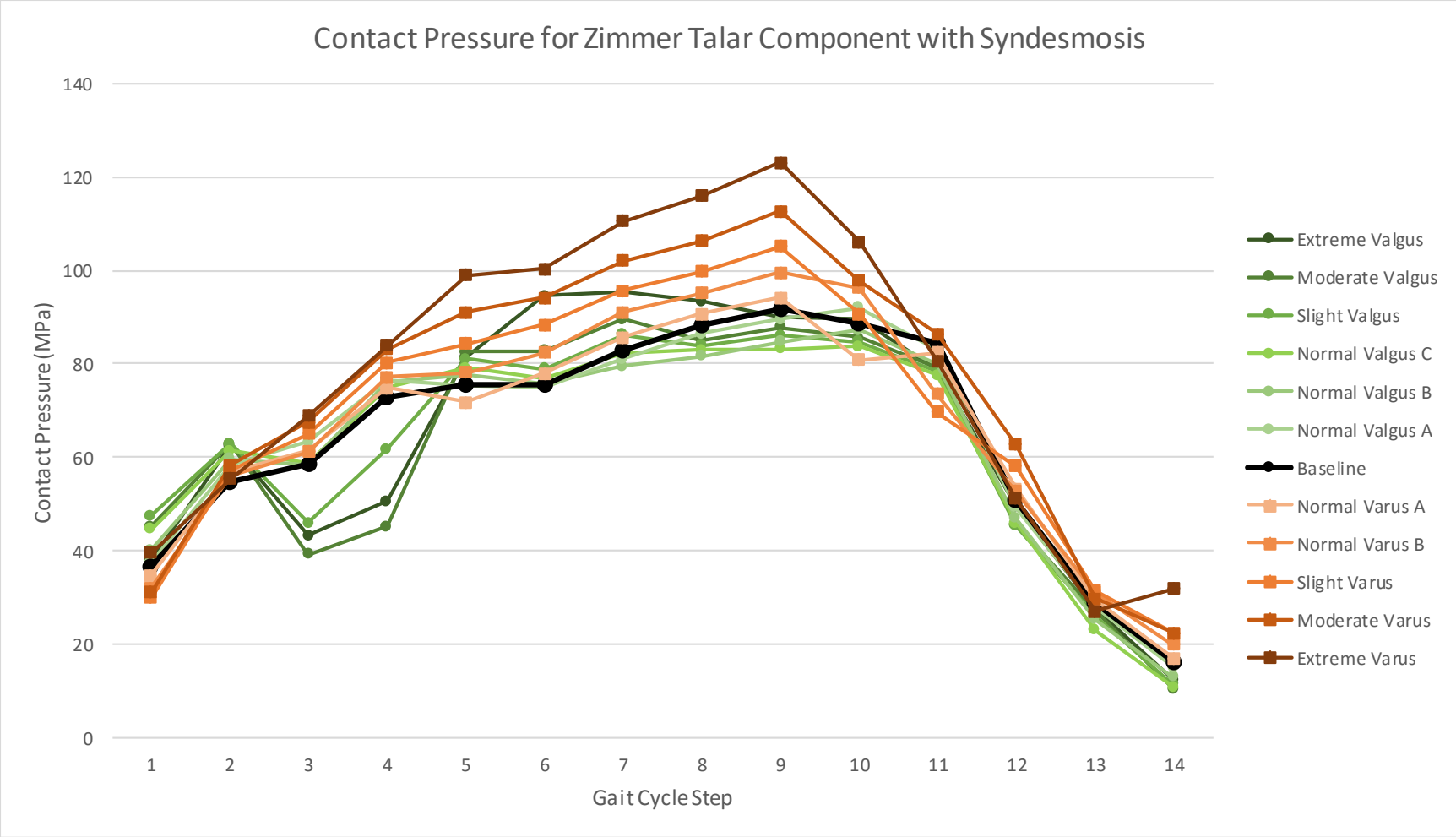

Figure 14. Maximum Contact Pressure for the Talar Component for the Zimmer TAA Model with Syndesmosis

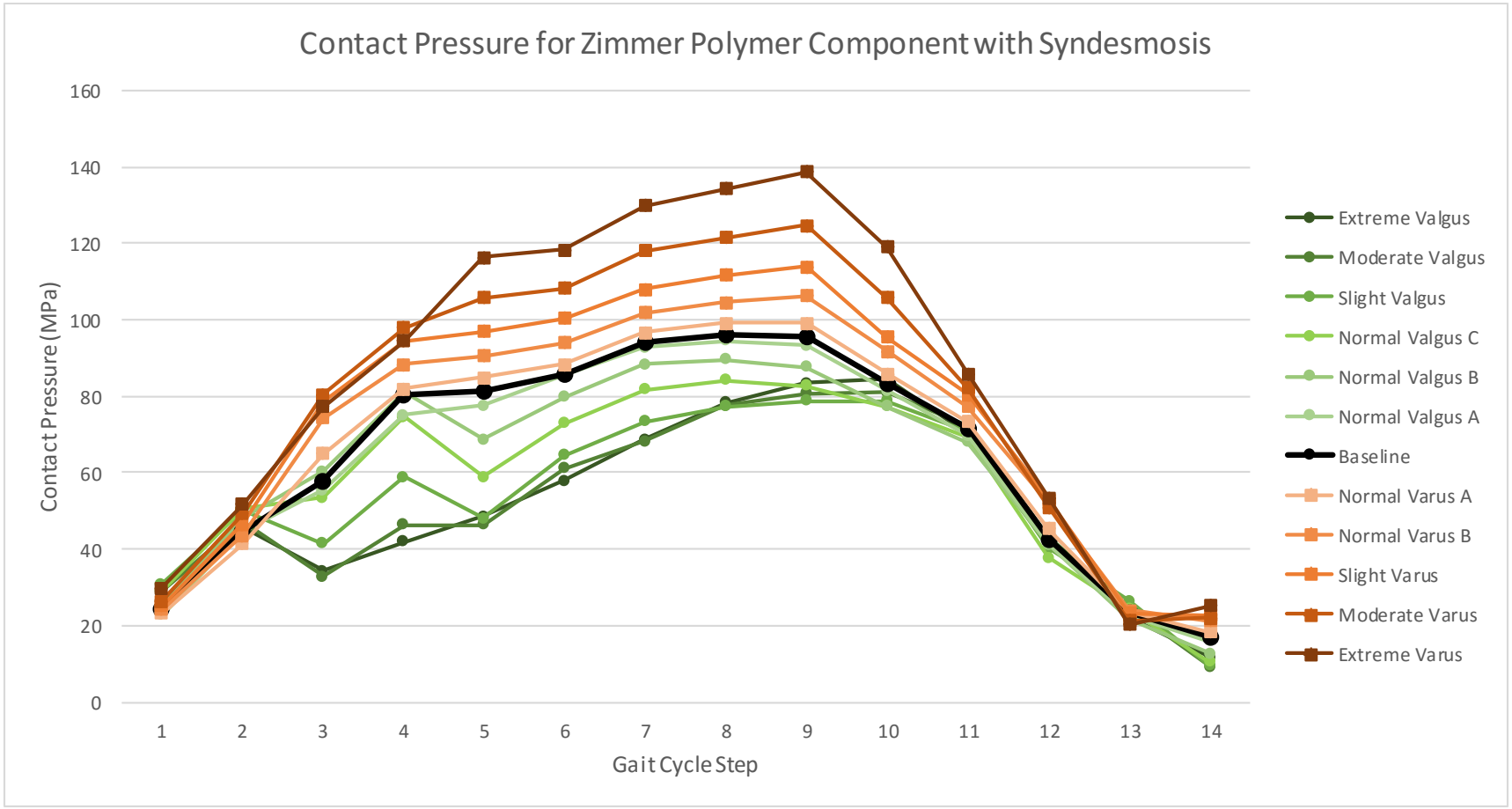

Figure 15. Maximum Contact Pressure for the Polymer Component for the Zimmer TAA Model with Syndesmosis

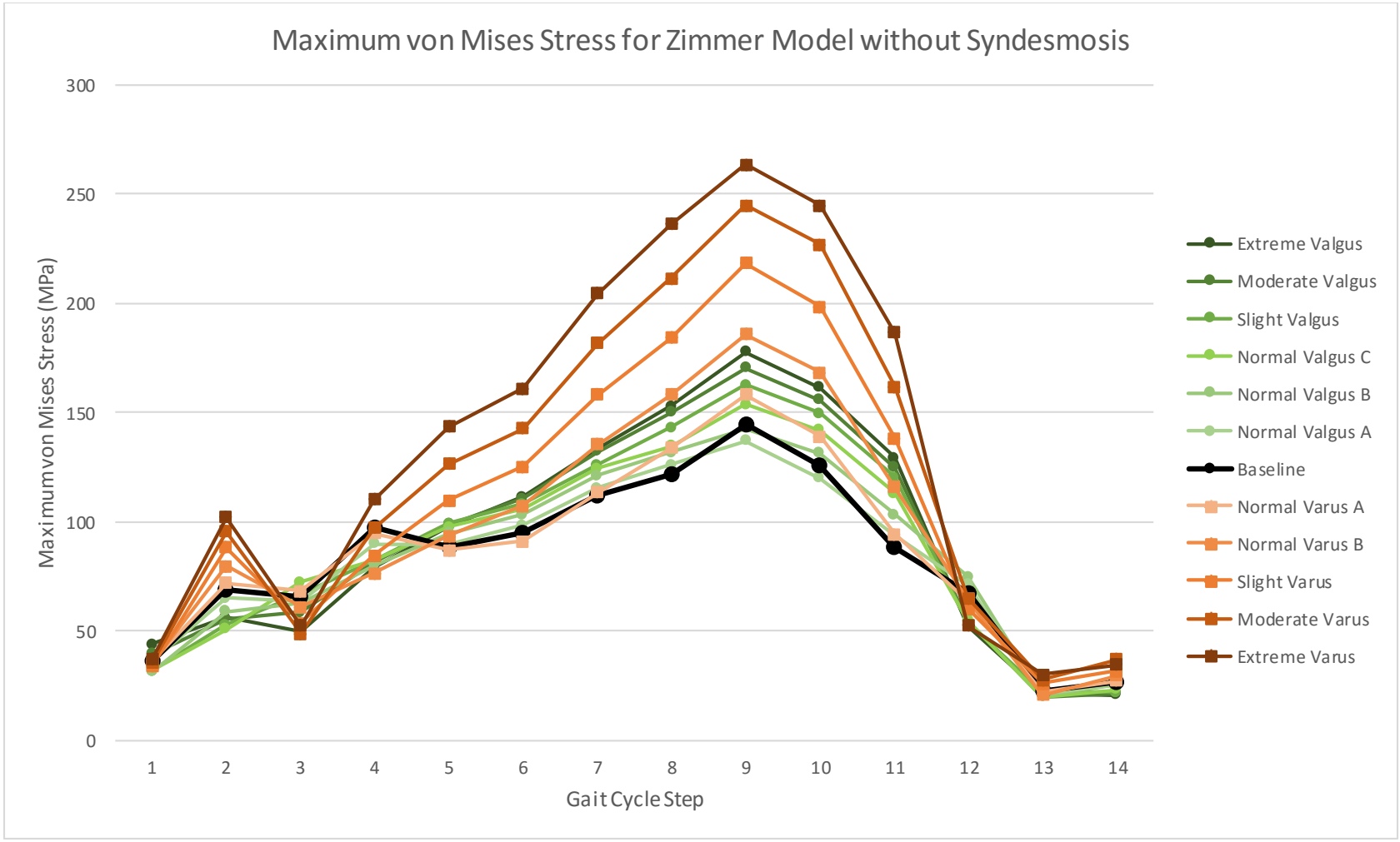

Figure 16. Maximum von Mises Stress for the End of Each Gait Cycle Step for the Zimmer TAA Model without Syndesmosis Ligaments

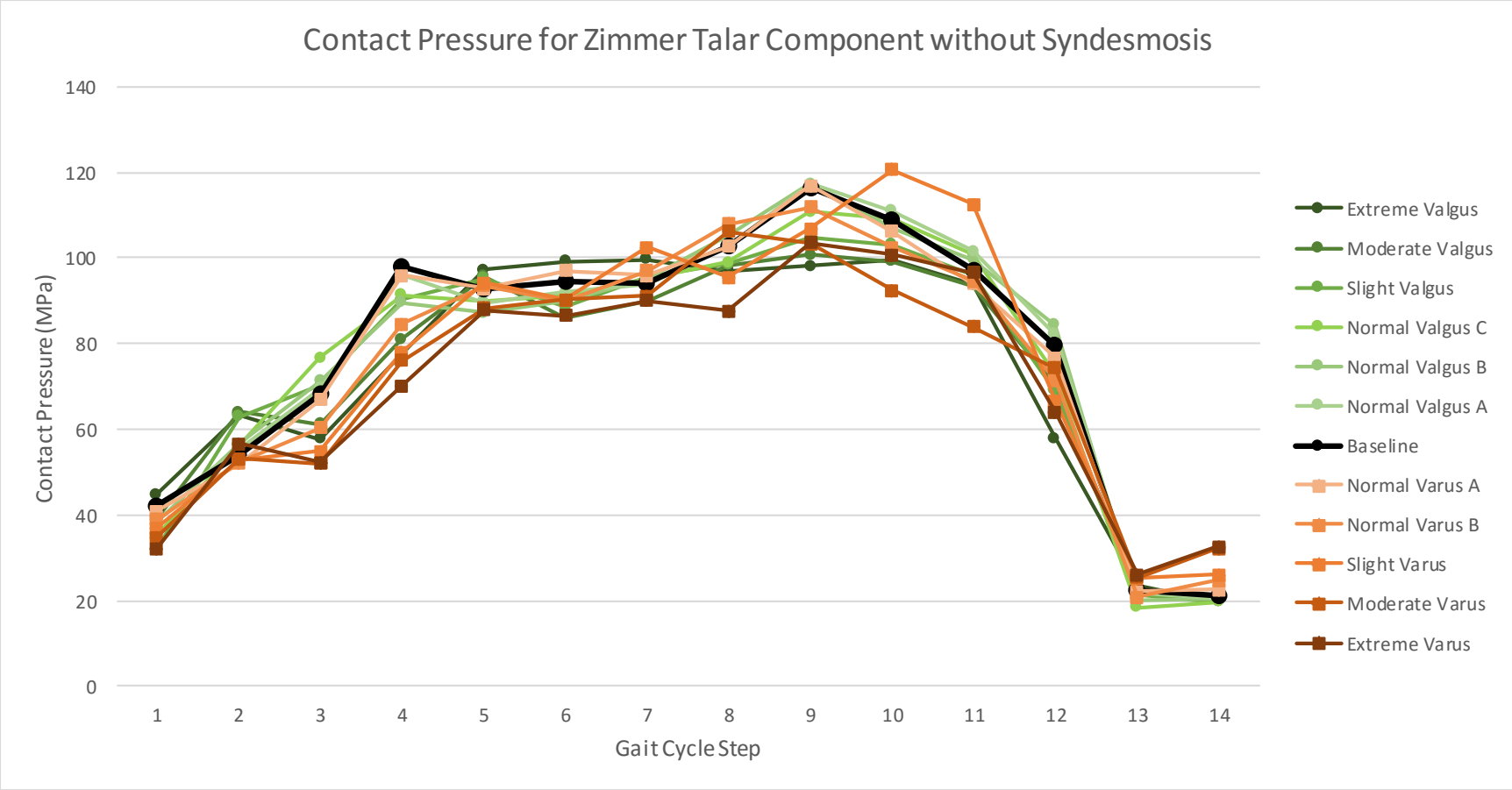

Figure 17. Maximum Contact Pressure for the Talar Component for the Zimmer TAA Model without Syndesmosis

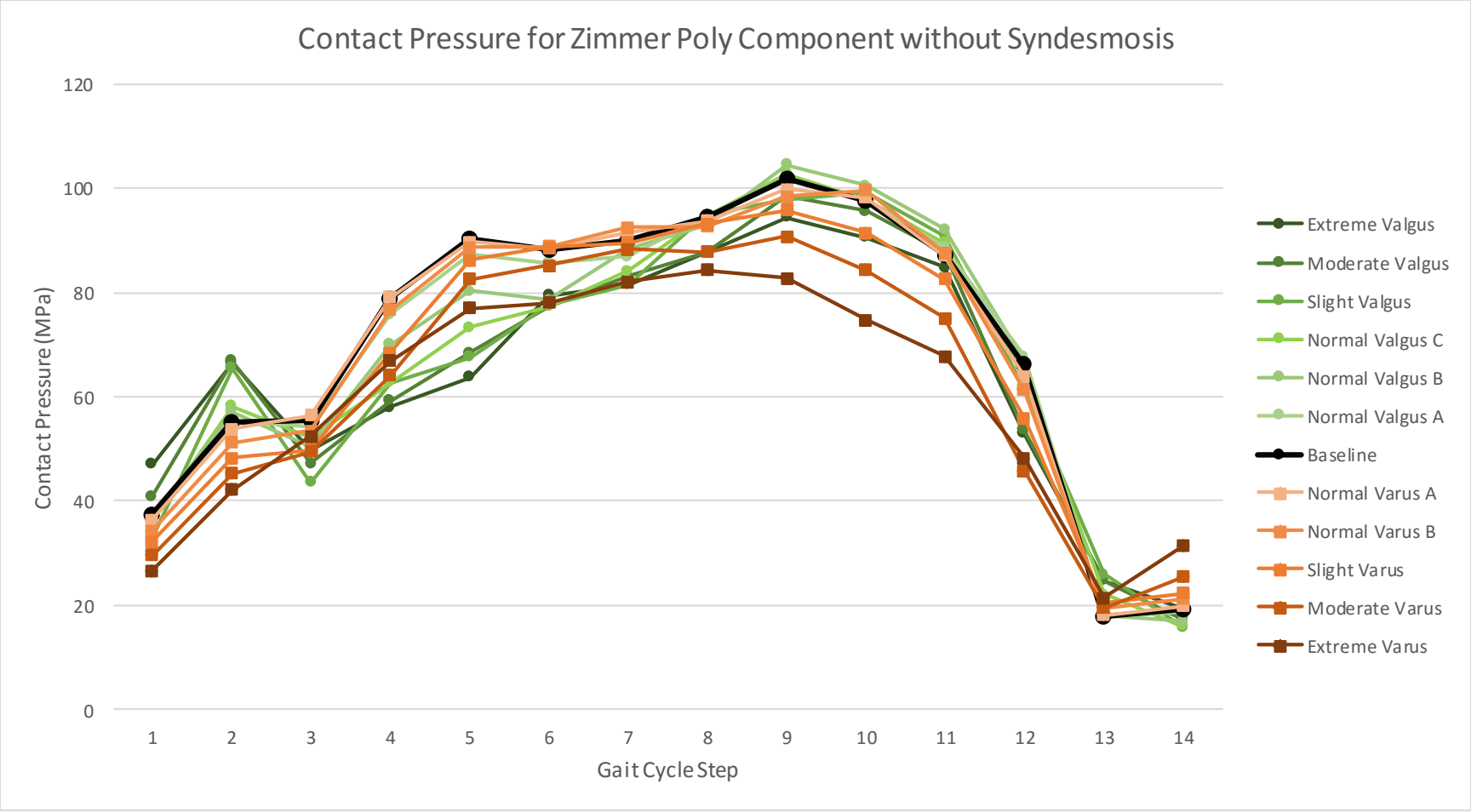

Figure 18. Maximum Contact Pressure for the Poly Component for the Zimmer TAA Model without Syndesmosis

STAR TAA

In the STAR model, the maximum stresses for the hardware components (omitting the bones) were collected at the completion of each step, and two surface contact pressure data sets were collected. Surface contact pressures were recorded separately for the interface between the bottom of the tibial component and top of the polymer bearing and the interface between the polymer component and the proximal side of the talar component. The STAR model was only run with the syndesmosis.

Overall, the stresses and contact pressures were much lower for the mobile-bearing STAR model than for the fixed-bearing Zimmer model. The maximum von Mises stresses in the STAR models occurred in the cylindrical rails and the keel of the tibial and talar components, respectively. The contact pressures in the STAR models were lower than for the Zimmer models and more distributed over the bearing surface. Maximum contact pressures on the distal articulation were consistently along the rail interface between the polymer bearing and the talar component. Instead of the varus alignments causing high stresses and contact pressures, as was the case for the Zimmer model, a valgus alignment created the highest stresses and contact pressures for the STAR implant. For the STAR, the varus models had the highest stresses and contact pressures during the early stance phase of gait, but during maximum loading during the gait cycle, the valgus models had the highest stress values. The dip in the maximum stress occurs at the beginning of the STAR model, similarly to the Zimmer, where the change in rotation occurs. Unlike the Zimmer, the STAR had contact between the fibula and the rest of the model toward the end of the gait cycle.

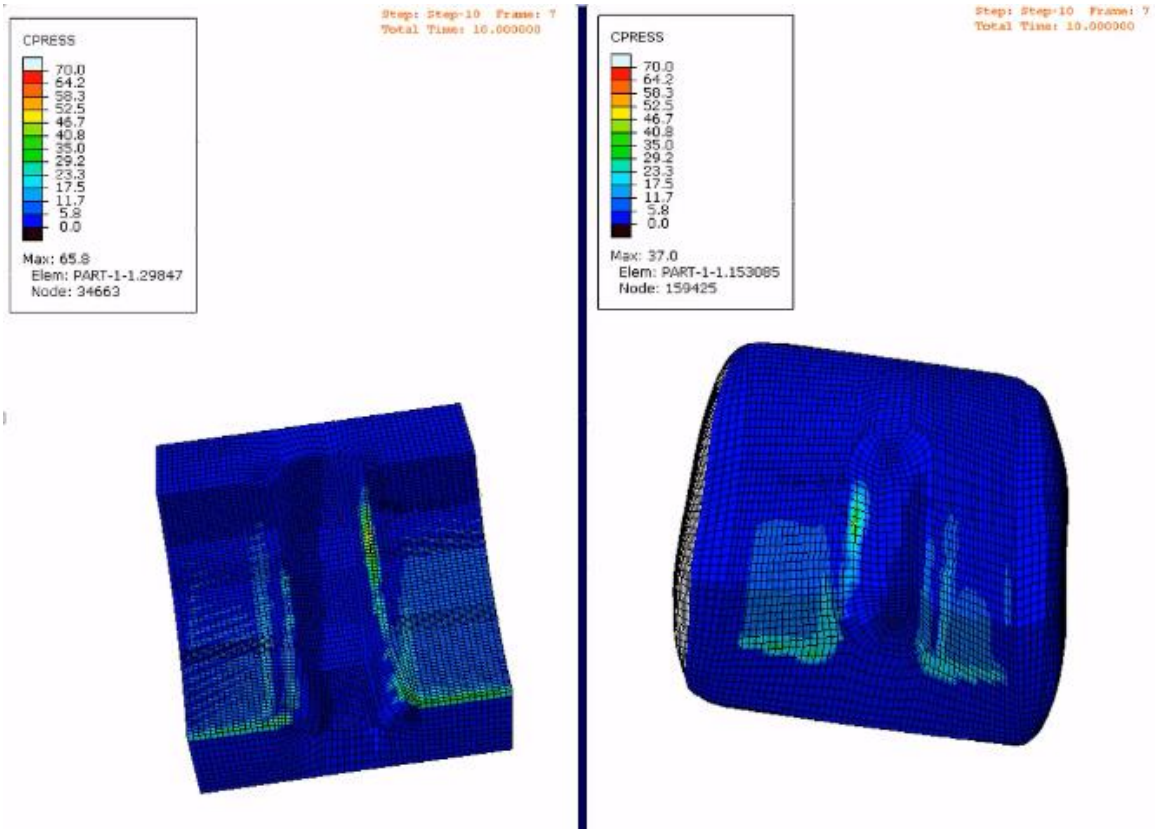

Figure 19. STAR Total Ankle contact pressure between polymer spacer (left) and talar component (right)

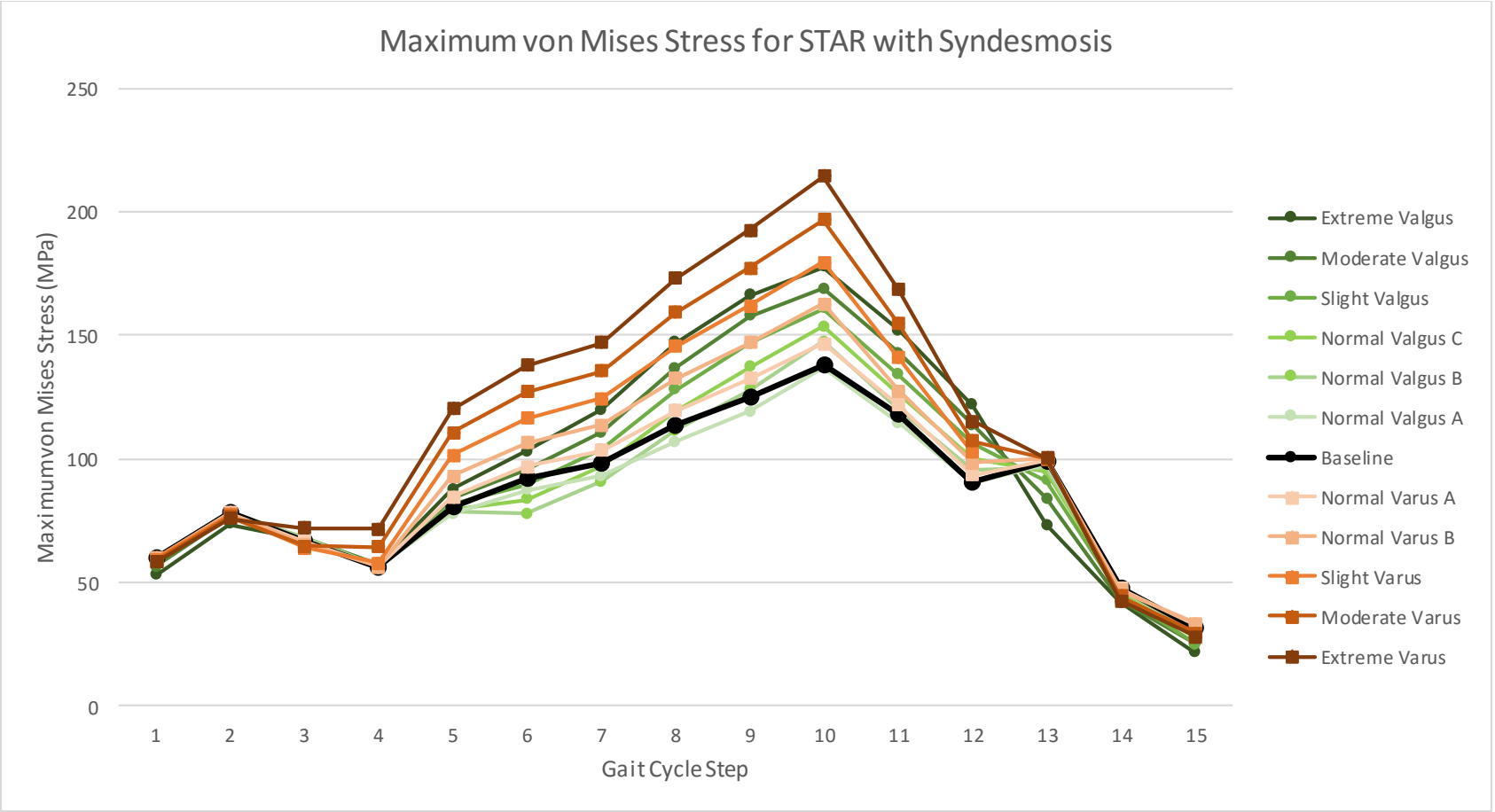

Figure 20. Maximum von Mises Stress for the STAR TAA Model with Syndesmosis Ligaments

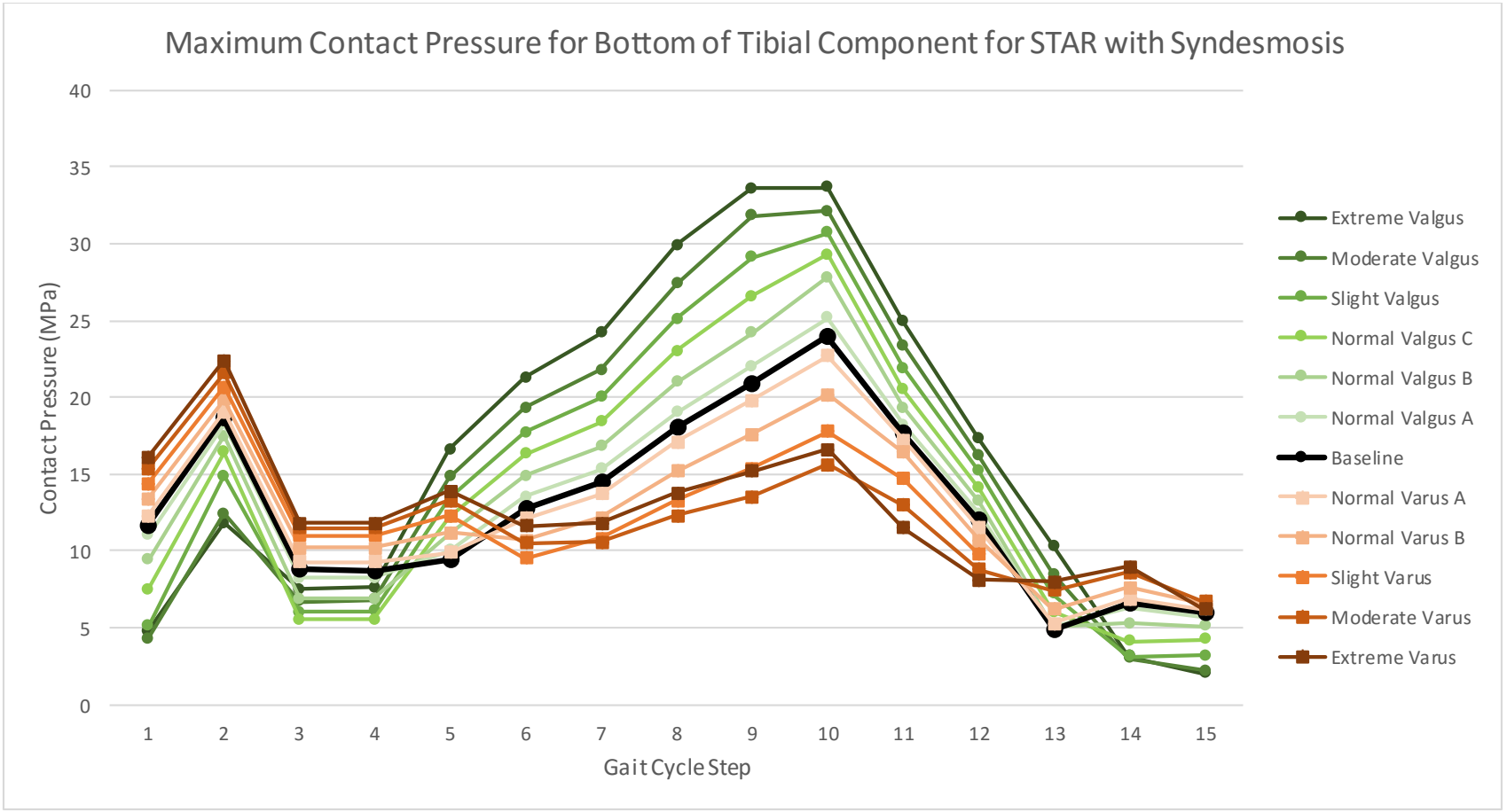

Figure 21. Maximum Contact Pressure for Bottom of Tibial Component for STAR with Syndesmosis

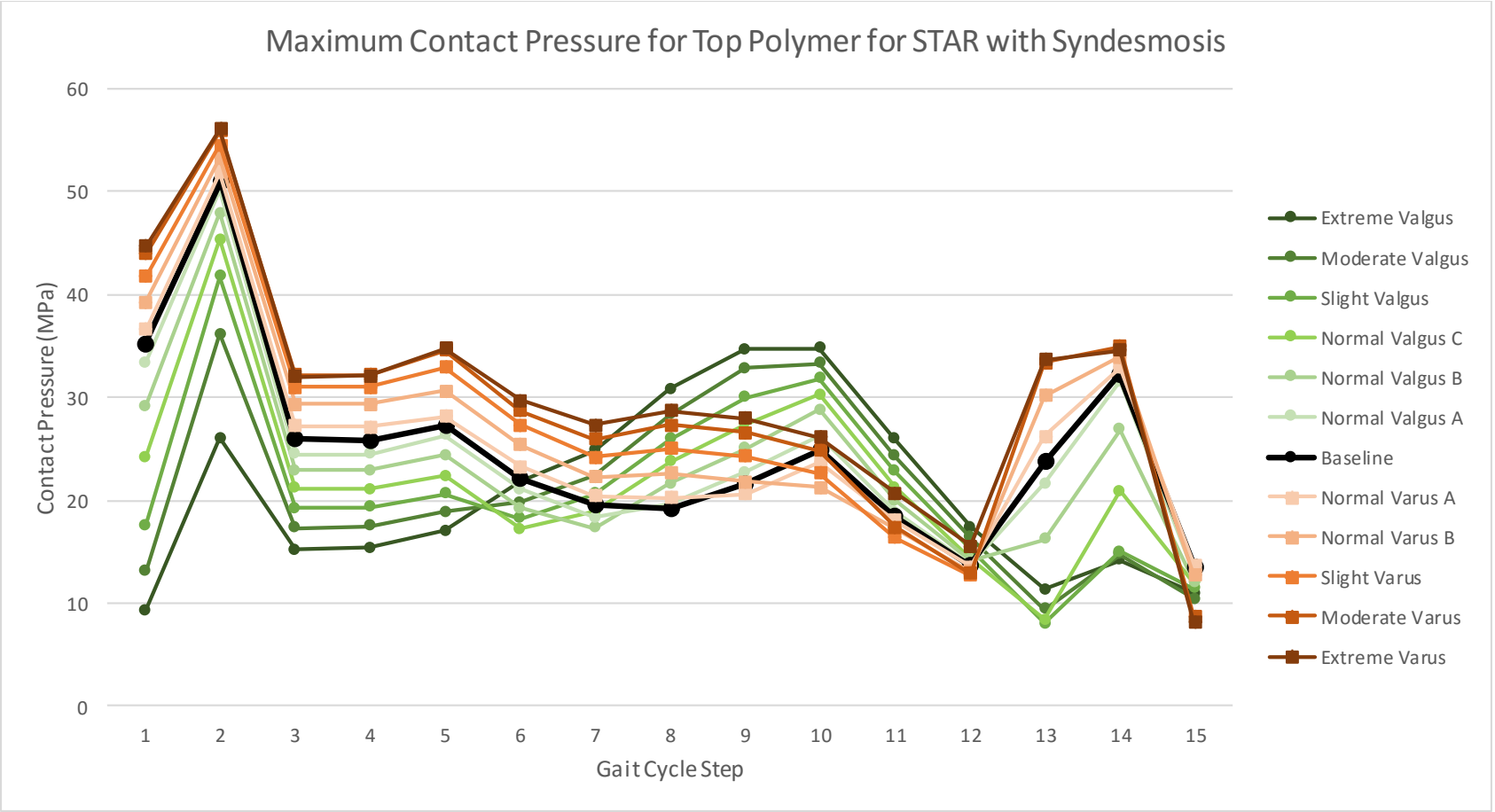

Figure 22. Maximum Contact Pressure for Top Polymer Component for STAR with Syndesmosis

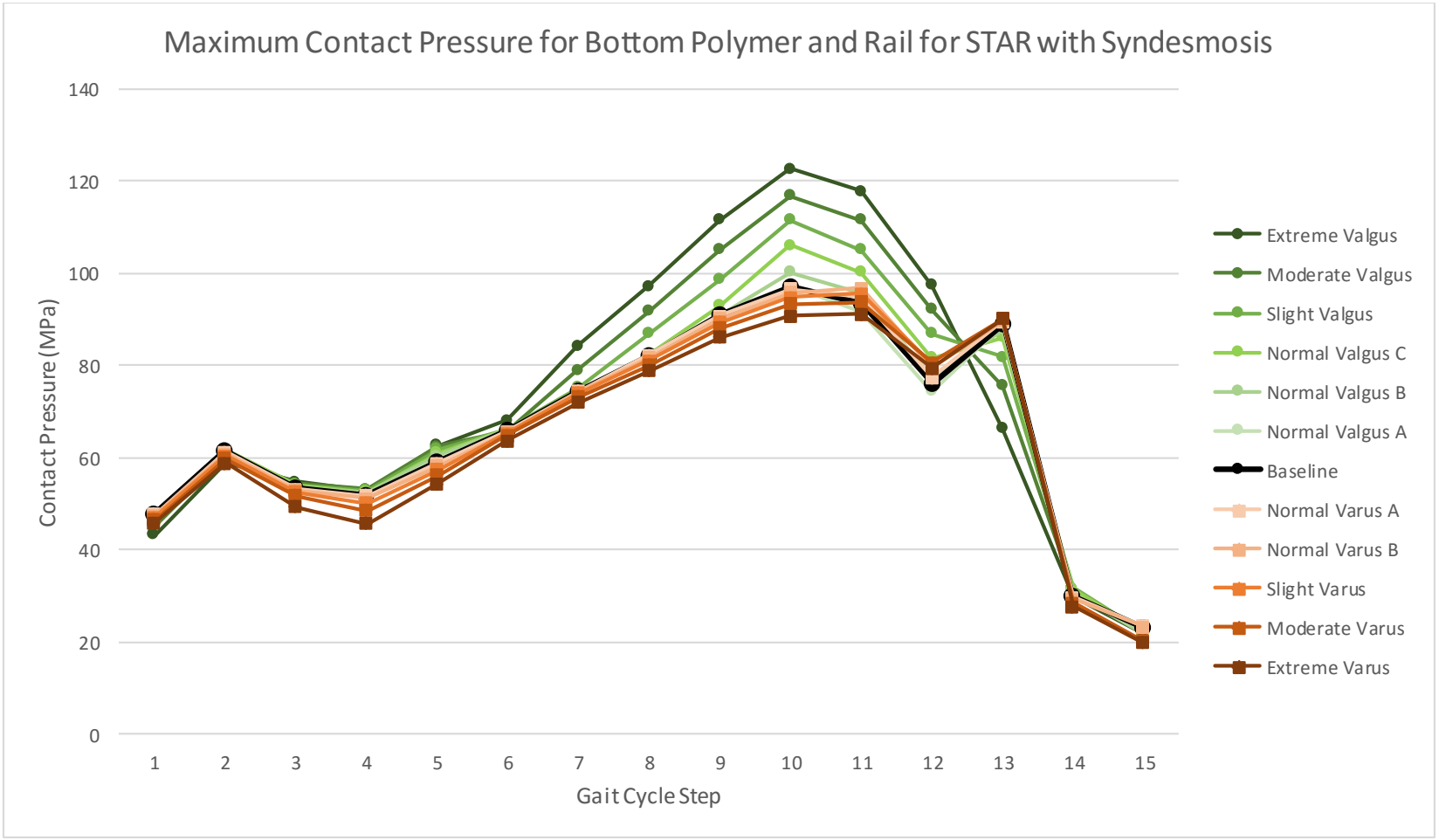

Figure 23. Maximum Contact Pressure for Bottom Polymer Component for STAR with Syndesmosis

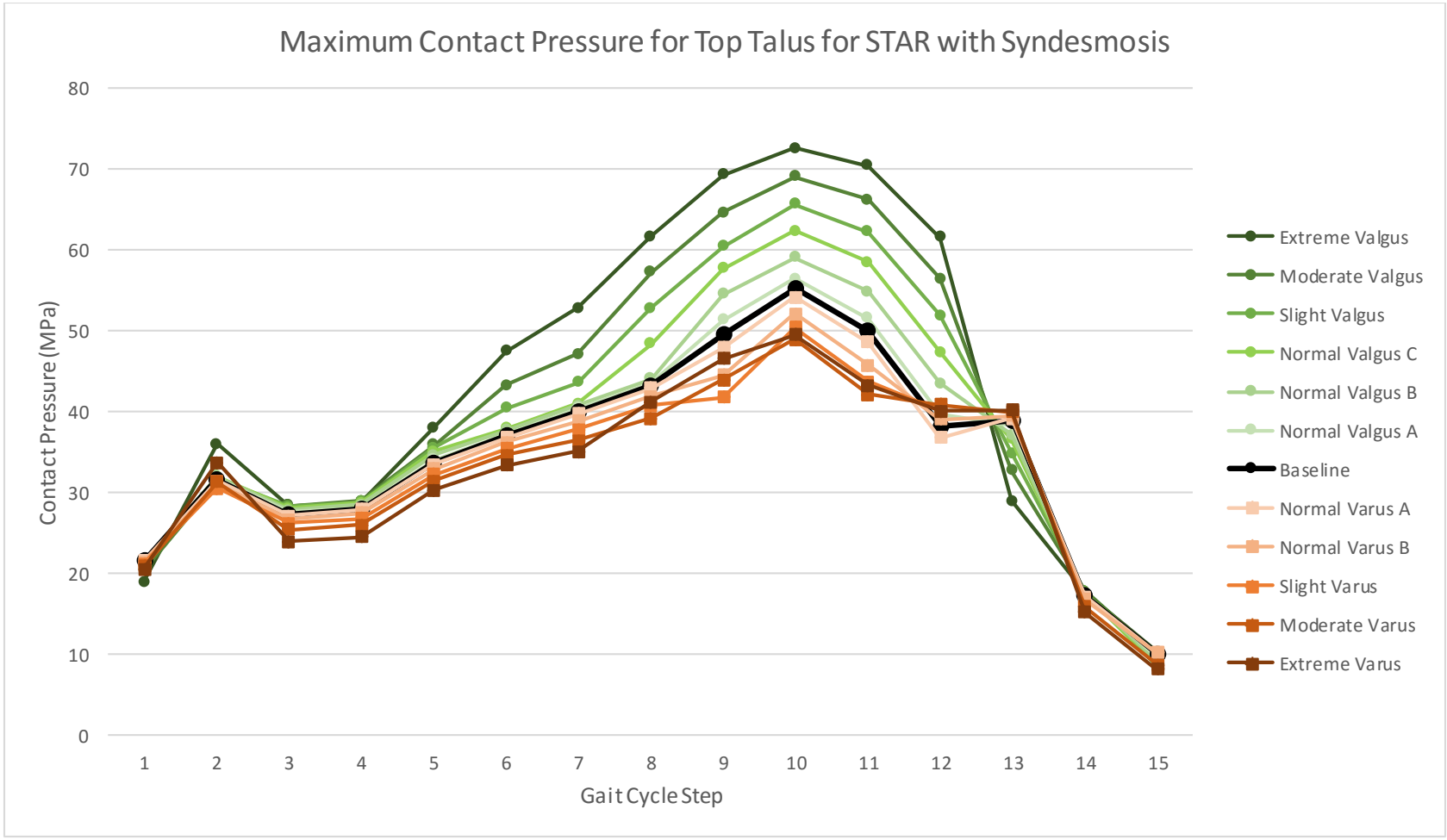

Figure 24. Maximum Contact Pressure for Top Talus component for STAR with Syndesmosis

CHAPTER 4: DISCUSSION

The purpose of this study was to determine how changes in the foot alignment alter stresses in the hardware of two TAA models, the STAR and the Zimmer. It was found that the STAR developed lower maximum stress values and contact pressure values regardless of foot alignment. The Zimmer models run with and without the syndesmosis showed that inclusion of a flexible syndesmosis produced larger maximum stress values and contact pressures in all foot alignments.

Both the stresses and the contact pressure curves of all the models and components correlate with the applied gait cycle forces, being consistent with heel-strike, roll-over, and toe-off. Interestingly, however, is the fact that the maximum stresses in the components were all located in the rails/cylinders of the tibial components. These are the attachment sites for the components to the bone. If these rails are under significant stress ingrowth of the bone could be negatively affected. This could lead to the components and bone not being fully integrated. The high stress occurring around the rail and bone interface could also lead to an increase in bone resorption which in turn could cause loosening of the implant. However, this model used only cortical bone material properties for the entire bone structure, and thus these stresses should not be over interpreted.

Directly comparing the maximum stresses for the Zimmer model with and without the syndesmosis modeled showed noteworthy differences in stresses. In the Zimmer model with the syndesmosis, the stresses may be higher due to the added resistance of the syndesmosis. Models for extreme varus and valgus were expected to have the highest stresses and contact pressures due to asymmetric bearing as the models potentially articulated on one side or the other. Interestingly, although the extreme varus

condition developed the highest stress for Zimmer models both with and without syndesmosis, rather counter-intuitively, the extreme varus model had the lowest contact pressure for the Zimmer model without the syndesmosis. And yet again, the highest contact pressure for the model with syndesmosis. Additionally, it is interesting to see that the for the Zimmer models both with and without syndesmosis, the extreme valgus model had one of the lowest contact pressures, and relatively low maximum stress in the models both with and without syndesmosis.

The contact pressures of the Zimmer implant in all hindfoot alignment models occurred on the domes of the bicondylar interfaces. Indeed, when evaluating the physical model qualitatively, the central sections of the components do not come into contact rather the domes of the talar component are the only regions of contact with the polymer bearing surface. This contact interface and the resultant stress patterns unfortunately may be an artifact of the source geometry. The Zimmer implant scanned to generate the model was not actual implantable hardware, but rather a plastic demo model. These contact patterns in the FE model accurately represented this demo articulation in which only the domes contact. However, the non-contacting center section does allow for the components to stay in place and rotate appropriately, which allows for some of the edge contact to be transferred inward. It is interesting that, even though the baseline healthy model had consistently low stresses and contact pressures, the "normal valgus" models were seen to have better outcomes than the "normal varus" models.

While it would have been ideal to generate the FE models from the actual geometry of the implants, as could be found in CAD models provided by the implant companies, this information was not available. Laser scanning and associated post-

processing potentially caused some inaccuracies in the resultant FE models. These inaccuracies were due to the need to laser scan the hardware which potentially led to slight inaccuracies due to reflectivity of the surfaces and resolution of the scanner. Due to smoothing required to merge the laser scans and geometric approximations made for ease of meshing, the geometries of the final FE models are not exactly the same as the original physical components. The hardware available for scanning was not necessarily the correct size for the bone models, meaning that sizing up or down of the components also had to be performed in the software in order to make the TAA fit the bone. It was challenging to make these virtual "cuts" in the model according to the surgical technique guide as the actual physical anatomy and surgical tools were absent. To improve accuracy of implantations, candidate implantations were reviewed by practicing foot and ankle surgeons to ensure the TAA was properly fit and oriented in the joint. The combination of slight vagaries in implant positioning and the bony material property approximation could have caused unusual peak stresses between the hardware components and the bone implantation interface. Even though the anatomical structures were necessary to investigate the question posed in this study, the focus was on the stresses and contact pressures of the components themselves, therefore the approximations and unusual peaks at the interfaces of the components and the bones are acceptable.

The use of springs to represent the ligaments were another limitation of this study. The springs allowed a more realistic rotation and movement in the ankle, and the springs were implanted at approximate locations on the bones to represent the insertion sites of the ligaments. These insertions initially were defined as a single node, but were changed to a two by two element set with the common surface node being the insertion

spot. This two by two element set was then pulled by the spring during the gait cycle. By allowing the two by two element set to be attached to the node, the pulling of the spring caused smaller stress elevations in those areas compared to the initial trial of having a single node represent the insertion spot. Because a calcaneus was not modeled, calcaneal insertions were placed at reference nodes which simulated the attachment sites on the calcaneus and were held in all directions.

Another limitation of not directly modeling the calcaneus was that the talus, which is typically supported distally by the calcaneus, was simply constrained not to move in the inferiorly (in the z-direction). In reality, the talus would be able to move a little in the downward z-direction against the calcaneus. This could change the amount of talar tilt that occurs in the model and potentially lower the high stresses and contact pressures of the hardware components.

Finally, during the last two increments, of the gait cycle, the compressive force had to be increased in order to maintain contact between the TAA surfaces. These last two increments are where toe-off occurs in the gait cycle leaving little to no compressive force except that of which the ligaments and muscular structures surrounding the bones and implants create. Thus, a slightly larger, negative, compressive force was applied, (-100N and -50N) which deviates from Stauffer's forces [1].

To further improve the anatomical realism of these FE models, the addition of more springs and a wider insertion area for the ligaments would be beneficial so high stresses peaks would not occur around attachment sites of the ligaments and to provide more realistic support of the ankle through the multiple ligaments. This could also be performed in replacing springs with continuum representations. The addition of the

calcaneus would also add the stability factor of having the bone structure that interacts most closely with the ground in the model. However, adding the calcaneus would increase the complexity of the model by adding additional surface interactions between the talus and tibia, adding elements of the mesh which would increase run time for the model, the ligaments which insert into the calcaneus would have an actual insertion point instead of simply being attached to a reference node which is held in space. Including the calcaneus could also give the opportunity to release some of the boundary conditions from the talus which would further help to replicate the actual movements of the tibia and talus. This would improve the models by further allowing the stabilizing ligaments to prevent rotation as well as to improve the realism of the gait cycle in an anatomical model. Obtaining computer aided design models for both the hardware models themselves as well as the surgical implantation cuts would also be beneficial for future studies as these would give better representations of the bones and the models themselves.

Though there were limitations, the overall study shows that the Zimmer has lower stresses and contact pressures in a valgus alignment. The STAR does not seem to favor either valgus or varus alignment, however, the STAR has significantly lower stresses and contact pressures compared to the Zimmer. This study shows that differences in surface articulations of TAAs and the alignment of the hindfoot have an effect on the stresses and contact pressures of the interfaces of the TAA.

APPENDIX A

Table A-1. Maximum Mises Stress for Zimmer TAA Model with Syndesmosis

Zimmer with Syndesmosis Mises Stress at End of Each Step														
Step	Rotation applied (radians)	Force applied (N)	Extreme Valgus (25mm)	Moderate Valgus (20mm)	Slight Valgus (15mm)	Normal Valgus C (10mm)	Normal Valgus B (5mm)	Normal Valgus A (0mm)	Baseline (-2.5mm)	Normal Varus A (-5mm)	Normal Varus B (-10mm)	Slight Varus (-15mm)	Moderate Varus (-20mm)	Extreme Varus (-25mm)
1	-0.061	-222.41	36.5	36.5	41.1	40.3	37.1	35	33.9	33.1	31.3	30.8	33.1	35.7
2	-0.07	-756.19	58.3	52.5	61.5	67.2	71.6	77.2	81.2	84.8	91.8	98.4	105	111.2
3	0	-756.19	49.2	49.6	53.4	54.9	53	54.5	51.7	54.9	60.1	61.8	63.5	64.1
4	0.014	-1512.39	91.3	90.4	90.9	86.4	83.4	79.5	78.5	77.5	92.1	106.9	122.6	139.7
5	0.056	-1734.80	115.8	113.5	110.1	104.6	100	95.1	96.2	105	123.7	142.7	163.2	186.3
6	0.086	-1823.77	126.9	123.3	119.8	113.3	108	102.7	110.6	120.2	140	161.4	183.7	205.3
7	0.096	-2250.79	145.3	140.7	136	128.6	122.4	129	141.3	153.2	177.7	203.6	233.3	252.5
8	0.11	-2535.48	160.3	153.8	148.6	140.5	133.8	151.3	165.2	178.7	206.9	236.2	257.4	280.7
9	0.131	-2829.06	178.4	168	159.7	153.7	147.8	177.7	193.2	208.6	238.8	259.4	277	325.9
10	0.155	-2197.42	168.4	154	147	144.2	139.3	139.2	151	163.1	188.6	215.7	239.2	270.8
11	0.16	-1378.94	118.4	118.2	107.1	113.3	110.8	108	106.5	104.5	113	129.5	148.5	175.5
12	0.105	-578.26	53.9	42.9	56.2	43.1	50.1	60.8	65.7	69.9	75.7	83.1	83.3	79.3
13	-0.035	-100	24.5	26.2	25.8	25.7	25.8	27.5	28.1	28.6	29.7	29.7	28.1	31.6
14	-0.096	-50	13.1	11.3	12.3	12	14.3	17.1	18.7	20.3	24.3	27.8	24.2	36.1

Table A-2. Maximum Contact Pressure for Valgus Alignments for the Talar and Tibial Components for the Zimmer TAA Model with Syndesmosis

Zimmer w/ Syndesmosis Max Contact Pressure (MPa)			Extreme Valgus (25mm)		Moderate Valgus (20mm)		Slight Valgus (15mm)		Normal Valgus C (10mm)		Normal Valgus B (5mm)		Normal Valgus A (0mm)	
Step	Rotation applied (radians)	Force applied (N)	Talar comp (MPa)	Tibial comp (MPa)	Talar comp (MPa)	Tibial comp (MPa)	Talar comp (MPa)	Tibial comp (MPa)	Talar comp (MPa)	Tibial comp (MPa)	Talar comp (MPa)	Tibial comp (MPa)	Talar comp (MPa)	Tibial comp (MPa)
1	-0.061	-222.411	37.8	26.4	45.1	28.9	47.4	31	44.6	29.2	40.2	25.1	37.5	22.8
2	-0.07	-756.1974	62.6	45.8	62.9	47	62.9	50.3	61.3	50.5	59.6	48	58.2	44.9
3	0	-756.1974	43.3	34.4	39.2	32.9	46	41.4	58.7	53.5	58.3	60.3	63.2	55.4
4	0.014	-1512.395	50.6	41.9	45.2	46.3	61.7	59	74.9	74.5	76	81.2	76.6	75.1
5	0.056	-1734.806	81.5	48.6	82.6	46.4	81.1	48	79.2	58.8	77.5	68.7	75.3	77.6
6	0.086	-1823.77	94.6	58	82.7	61	79	64.6	76.8	73	75.6	79.8	75.1	85.6
7	0.096	-2250.799	95.5	68.6	89.5	68.3	86.3	73.5	82.4	81.7	79.5	88.3	81	92.9
8	0.11	-2535.485	93.3	78.2	85.1	77.5	83.9	77.3	82.9	84.3	81.7	89.7	86.4	94.6
9	0.131	-2829.068	90	83.4	87.8	80.8	86.1	78.7	83.2	82.7	84.7	87.7	89.6	93.3
10	0.155	-2197.421	89.5	84.6	85.7	80.9	84.7	78.8	83.7	77.4	87.3	77.2	92.1	81.5
11	0.16	-1378.948	78.8	70.3	79.2	72.2	78.5	70.8	77.5	69.5	80	68.1	83.2	69.8
12	0.105	-578.2686	49.5	41.6	45.6	43.5	45.3	40.2	46	37.7	46.9	41.1	49.2	41.5
13	-0.035	-100	27.5	22.1	27.2	24.6	25.8	26.4	23	24.2	25.3	21.6	27.8	22.8
14	-0.096	-50	12.3	11.7	10.4	9.2	11.4	9.6	10.9	10.6	12.9	12.6	15.1	15.9

Table A-3. Maximum Contact Pressure for Baseline and Varus Alignments for the Talar and Tibial Components for the Zimmer TAA Model with Syndesmosis

Zimmer w/ Syndesmosis Max Contact Pressure (MPa)			Baseline (-2.5mm)		Normal Varus A (-5mm)		Normal Varus B (-10mm)		Slight Varus (-15mm)		Moderate Varus (-20mm)		Extreme Varus (-25mm)	
Step	Rotation applied (radians)	Force applied (N)	Tibial comp (MPa)	Tibial comp (MPa)	Talar comp (MPa)	Tibial comp (MPa)	Talar comp (MPa)	Tibial comp (MPa)	Talar comp (MPa)	Tibial comp (MPa)	Talar comp (MPa)	Tibial comp (MPa)	Talar comp (MPa)	Tibial comp (MPa)
1	-0.061	-222.411	36.7	24.2	34.7	23.2	32	24.2	29.9	25.2	31	26.5	39.5	29.8
2	-0.07	-756.1974	54.6	44.5	56.7	41.5	55.9	43.6	57.2	46.6	58.2	49.4	55.3	51.7
3	0	-756.1974	58.7	57.7	61.4	65.1	61.2	74.3	65.1	78.8	67.6	80.6	68.8	77.3
4	0.014	-1512.395	72.8	80.3	74.9	81.9	77.2	88.4	80.2	94.4	83.1	97.9	83.9	94.6
5	0.056	-1734.806	75.4	81.4	71.8	85	78.2	90.7	84.3	97	91	105.9	99	116.5
6	0.086	-1823.77	75.5	86	77.9	88.4	82.3	94	88.3	100.5	94.1	108.3	100.4	118.3
7	0.096	-2250.799	82.8	94	85.6	96.8	91.1	101.8	95.6	108.1	102	118	110.5	129.9
8	0.11	-2535.485	88.4	96.2	90.7	99.2	95.2	104.6	99.8	111.7	106.3	121.6	116	134.4
9	0.131	-2829.068	91.8	95.7	94.2	99.2	99.5	106.3	105.2	113.9	112.7	124.7	123	138.7
10	0.155	-2197.421	88.5	83.3	80.9	85.8	96.2	91.7	90.6	95.5	97.8	105.9	106.1	119
11	0.16	-1378.948	84.6	71.4	82.4	73.3	73.5	77.4	69.7	80.5	86.4	82.3	80.6	86
12	0.105	-578.2686	50.9	42.4	53.3	45.4	52.6	51.9	58.1	52.9	62.7	51.1	51.1	53.5
13	-0.035	-100	28.7	23.3	29.5	23.5	31	24	31.4	23.3	29.8	21.2	27	20.4
14	-0.096	-50	16.2	17.2	17.1	18.3	20	21.2	22.4	22.7	22.5	22.1	31.9	25.3

Table A-4. Maximum Mises Stress for Zimmer TAA Model without Syndesmosis

Zimmer without Syndesmosis Mises Stress at End of Each Step														
Step	Rotation applied (radians)	Force applied (N)	Extreme Valgus (25mm)	Moderate Valgus (20mm)	Slight Valgus (15mm)	Normal Valgus C (10mm)	Normal Valgus B (5mm)	Normal Valgus A (0mm)	Baseline (-2.5mm)	Normal Varus A (-5mm)	Normal Varus B (-10mm)	Slight Varus (-15mm)	Moderate Varus (-20mm)	Extreme Varus (-25mm)
1	-0.061	-222.411	43.9	39.4	31.6	31.9	31.4	35.9	36.6	36.1	34.8	33.8	35.4	37
2	-0.07	-756.1974	56	55.7	52.9	50.8	58.7	64.9	68.7	71.9	79.8	88	95.4	102
3	0	-756.1974	49.6	58.4	66.6	72.4	62.9	63.7	65.5	68.4	60.8	53.7	48.9	52.5
4	0.014	-1512.395	79.2	81.5	82.2	81.9	80.1	89.7	97.3	94.6	76.5	84.3	97.3	110.1
5	0.056	-1734.806	97.7	98.7	99.3	97.7	94.8	89.9	88	86.8	93.5	109.7	126.3	143.6
6	0.086	-1823.77	111.5	110.4	108.1	106.2	103.2	98.2	94.9	91	107.2	125.1	142.7	161
7	0.096	-2250.799	133.6	132	125.9	124.2	121	115.4	111.7	113.5	135.2	158.1	181.9	204.7
8	0.11	-2535.485	152.8	150.1	143	134.5	131.6	126	122.1	133.7	158.2	184.3	211.5	236.3
9	0.131	-2829.068	177.5	170.4	162.7	153.5	142.5	137	144.6	158.1	185.8	218.5	244.8	263.5
10	0.155	-2197.421	161.4	155.6	149.6	141.7	131.3	119.7	126	139	168.4	198.4	226.8	244.7
11	0.16	-1378.948	129.2	124.9	120.2	112.9	103.2	93.5	88	94.4	115.9	138.2	161.8	186.6
12	0.105	-578.2686	52.4	54.3	53.8	54.7	74.8	71	67.3	63.8	64.5	60.2	64.9	52.2
13	-0.035	-100	21.6	20	22.3	19.8	20.5	21.6	22.5	22.1	20.6	26.1	27.6	29.8
14	-0.096	-50	20.8	21.6	21.8	22.9	25.4	25.4	26.2	27.1	29.5	31.5	36.8	34.3

Table A-5. Maximum Contact Pressure for Valgus Alignments for the Talar and Tibial Component for the Zimmer TAA Model without Syndesmosis

Zimmer w/o Syndesmosis Max Contact Pressure (MPa)			Extreme Valgus (25mm)		Moderate Valgus (20mm)		Slight Valgus (15mm)		Normal Valgus C (10mm)		Normal Valgus B (5mm)		Normal Valgus A (0mm)	
Step	Rotation applied (radians)	Force applied (N)	Talar comp (MPa)	Tibial comp (MPa)	Talar comp (MPa)	Tibial comp (MPa)	Talar comp (MPa)	Tibial comp (MPa)	Talar comp (MPa)	Tibial comp (MPa)	Talar comp (MPa)	Tibial comp (MPa)	Talar comp (MPa)	Tibial comp (MPa)
1	-0.061	-222.411	44.8	47.1	39.4	41	32.2	33	35.2	36.1	38.5	37.1	41.6	37.4
2	-0.07	-756.1974	63.3	66.5	64.1	66.9	63	65.6	56.3	58.2	56.6	57.1	55.2	55.5
3	0	-756.1974	57.8	49.8	61.3	47.3	70.2	43.6	76.7	52.2	71.2	50.5	69.6	54.2
4	0.014	-1512.395	77.9	58.1	81	59.3	90.3	62.7	91.3	62.8	89.6	70	96	75.8
5	0.056	-1734.806	97.2	63.8	95.7	68.5	95.3	67.6	89.8	73.4	87.2	80.4	89.5	87.3
6	0.086	-1823.77	99.2	79.4	86	77.3	88.4	77.6	91.3	77.4	90.1	78.5	91.9	85.7
7	0.096	-2250.799	99.6	81.6	89.9	83.3	95.8	81.5	95.3	84.2	95	88.5	93.9	86.9
8	0.11	-2535.485	97	87.6	98.3	87.7	98.6	95	98.9	94.6	105	92.9	102.5	94.8
9	0.131	-2829.068	98.1	94.4	100.7	98.4	104.9	98	110.7	102.8	117.4	104.6	117.4	102
10	0.155	-2197.421	99.4	90.6	99.1	95.6	103.2	99.1	109	98	106.8	100.6	111.1	97.9
11	0.16	-1378.948	94	84.8	93.6	87.9	95.9	90.9	100.8	89.6	99.7	92.1	101.7	88.7
12	0.105	-578.2686	58	52.9	70.2	53.7	69.1	61.5	73	64	84.3	66.7	82.1	67.8
13	-0.035	-100	23.6	24.7	22.1	24.7	21.2	26	18.5	22.1	20.1	18	21.8	17.8
14	-0.096	-50	19.8	19.3	20	17.5	19.6	15.8	19.6	16.1	20.4	17	20.3	18.7

Table A-6. Maximum Contact Pressure for Baseline and Varus Alignments for the Talar and Tibial Components for the Zimmer TAA Model without Syndesmosis

Zimmer w/o Syndesmosis Max Contact Pressure (MPa)			Baseline (-2.5mm)		Normal Varus A (-5mm)		Normal Varus B (-10mm)		Slight Varus (-15mm)		Moderate Varus (-20mm)		Extreme Varus (-25mm)	
Step	Rotation applied (radians)	Force applied (N)	Talar comp (MPa)	Tibial comp (MPa)	Talar comp (MPa)	Tibial comp (MPa)	Talar comp (MPa)	Tibial comp (MPa)	Talar comp (MPa)	Tibial comp (MPa)	Talar comp (MPa)	Tibial comp (MPa)	Talar comp (MPa)	Tibial comp (MPa)
1	-0.061	-222.411	41.9	37.3	41	36.4	39	34.3	37	32.2	34.7	29.6	32.2	26.7
2	-0.07	-756.1974	54.1	55	52.1	53.8	52.2	51.2	53	48.2	53.2	45.3	56.7	42.1
3	0	-756.1974	68.3	55.5	66.8	56.4	60.4	53.5	54.8	49.8	52	49.5	52.2	52.4
4	0.014	-1512.395	97.8	78.7	95.9	79.1	84.6	76.7	78	68.4	76.1	64.1	70.2	66.9
5	0.056	-1734.806	92.6	90.2	92.9	89.7	93.6	88.6	94.1	86.2	88.2	82.6	87.9	77
6	0.086	-1823.77	94.4	88.3	97	88.5	90.1	88.9	90.2	88.7	90.3	85.2	86.5	78
7	0.096	-2250.799	94	89.9	95.9	91.7	97.1	92.6	102.5	89.6	91.1	88.3	90	82
8	0.11	-2535.485	102.8	94.5	102.7	93.8	108	92.7	95.5	93.2	106.3	87.8	87.7	84.3
9	0.131	-2829.068	116.3	101.8	117	99.9	111.8	98.4	106.8	95.9	103.4	90.8	103.6	82.7
10	0.155	-2197.421	108.9	97.6	106.1	98.3	102.4	99.7	120.7	91.4	92.4	84.3	100.8	74.8
11	0.16	-1378.948	97	87.1	93.9	87.2	94.6	87.6	112.6	82.6	83.9	75.1	96.5	67.7
12	0.105	-578.2686	79.5	66.4	76.7	64	71.4	61.4	66.6	56	74.3	45.9	64	48.2
13	-0.035	-100	22.5	17.9	22.1	18.2	20.9	19.5	25.2	20.6	25.3	19.6	26.1	21.4
14	-0.096	-50	21.2	19.3	22.6	19.9	24.8	21.2	26.1	22.4	32.1	25.5	32.7	31.4

Table A-7. Maximum Stress for STAR Hardware Components

STAR with Syndesmosis Mises Stress at End of Each Step														
Step Number	Rotation applied (radians)	Force applied (N)	Extreme Valgus	Moderate Valgus	Slight Valgus	Normal Valgus C	Normal Valgus B	Normal Valgus A	Baseline	Normal Varus A	Normal Varus B	Slight Varus	Moderate Varus	Extreme Varus
1	-0.061	-222.411	53	56.5	58.3	59.3	59.8	60	60	60	59.8	59.4	58.8	58.2
2	-0.07	-756.1974	73.8	76.4	77.8	78.3	78.5	78.4	78.3	78.2	77.8	77.3	76.7	75.8
3	-0.03	-756.2	67.3	67.9	68.1	68	67.8	67.3	67	66.7	65.7	64	64.8	72.2
4	0	-756.1974	57.1	57.1	56.8	56.5	56.4	56.4	56.4	56.3	56.3	57.8	64.4	71.7
5	0.014	-1512.395	87.8	84.5	81.8	79.7	78.7	77.8	80.7	84.8	93.1	101.7	110.7	120.3
6	0.056	-1734.806	103.1	95.7	89.5	83.5	78	87.3	92.1	96.9	106.6	116.6	127.1	138
7	0.086	-1823.77	120	110.6	103.8	97.3	90.9	93.1	98.2	103.3	113.7	124.5	135.7	147.2
8	0.096	-2250.799	147.1	136.7	127.8	119.5	111.5	107.1	113.4	119.7	132.5	145.6	159.2	173.2
9	0.11	-2535.485	166.4	157.9	146.6	137.1	127.9	119	125.4	132.6	147.1	161.9	177.2	192.8
10	0.131	-2829.068	177.7	169.1	161	153.5	147.4	137.2	138.5	146.6	162.9	179.6	196.8	214.3
11	0.155	-2197.421	152	142.9	134.1	126.2	120.1	114.5	118.3	121.8	127.7	141.1	154.7	168.6
12	0.16	-1378.948	121.7	113.8	106.7	100.6	95.3	90	90.8	93.6	98.7	102.8	107.3	115.3
13	0.105	-578.2686	73.3	83.9	91.1	95.2	96.6	98.3	99	99.5	100		100.2	100.3
14	-0.035	-100	41.7	42.7	44.9	46.7	47.5	47.8	47.8	47.6	47		44.7	42.8
15	-0.096	-50	21.6	25	25	27.2	29.1	31.1	32.1	33	33.4		29.7	28.1

Table A-84. Maximum Contact Pressure for STAR Tibial Component

STAR Contact Pressure for Tibial Component														
Step Number	Rotation applied (radians)	Force applied (N)	Extreme Valgus	Moderate Valgus	Slight Valgus	Normal Valgus C	Normal Valgus B	Normal Valgus A	Baseline	Normal Varus A	Normal Varus B	Slight Varus	Moderate Varus	Extreme Varus
1	-0.061	-222.411	4.8	4.3	5.1	7.5	9.4	11	11.6	12.3	13.4	14.4	15.4	16.1
2	-0.07	-756.1974	11.8	12.4	14.9	16.4	17.5	18.3	18.7	19.1	19.9	20.7	21.6	22.4
3	-0.03	-756.2	7.5	6.7	6	5.5	6.9	8.2	8.8	9.3	10.2	11	11.5	11.8
4	0	-756.1974	7.6	6.8	6.1	5.5	6.9	8.2	8.7	9.3	10.2	11	11.5	11.8
5	0.014	-1512.395	16.6	14.8	13.4	12.2	11.1	10	9.4	9.9	11.2	12.3	13.3	13.9
6	0.056	-1734.806	21.3	19.3	17.7	16.3	14.9	13.5	12.8	12.1	10.7	9.5	10.5	11.6
7	0.086	-1823.77	24.2	21.8	20	18.4	16.8	15.3	14.5	13.7	12.2	10.8	10.6	11.8
8	0.096	-2250.799	29.9	27.4	25.1	23	21	19	18.1	17.1	15.2	13.3	12.3	13.8
9	0.11	-2535.485	33.6	31.8	29.1	26.6	24.2	22	20.9	19.8	17.6	15.4	13.5	15.2
10	0.131	-2829.068	33.7	32.1	30.7	29.3	27.8	25.2	24	22.7	20.2	17.8	15.6	16.6
11	0.155	-2197.421	24.9	23.4	21.9	20.5	19.3	18.2	17.7	17.2	16.4	14.7	13	11.5
12	0.16	-1378.948	17.3	16.2	15.2	14.1	13.2	12.4	12	11.5	10.7	9.8	8.8	8.1
13	0.105	-578.2686	10.3	8.5	7.2	6	5.1	5	4.9	5.3	6.2		7.4	8
14	-0.035	-100	3.1	3	3.1	4.1	5.3	6.3	6.6	6.9	7.6		8.6	9
15	-0.096	-50	2	2.2	3.2	4.2	5.1	5.7	6	6.2	6.5		6.7	6.2

Table A-9. Maximum Contact Pressure for Top of STAR Polymer Component

STAR Contact Pressure for Top Polymer Component														
Step Number	Rotation applied (radians)	Force applied (N)	Extreme Valgus	Moderate Valgus	Slight Valgus	Normal Valgus C	Normal Valgus B	Normal Valgus A	Baseline	Normal Varus A	Normal Varus B	Slight Varus	Moderate Varus	Extreme Varus
1	-0.061	-222.411	9.3	13.1	17.6	24.2	29.2	33.4	35.1	36.6	39.3	41.7	43.9	44.7
2	-0.07	-756.1974	26	36.1	41.7	45.3	47.9	50.1	51	51.8	53.2	54.5	55.9	56.1
3	-0.03	-756.2	15.2	17.3	19.2	21.2	22.9	24.5	25.9	27.2	29.3	31	32.2	32
4	0	-756.1974	15.4	17.5	19.3	21.1	22.9	24.5	25.8	27.1	29.3	31	32.2	32.1
5	0.014	-1512.395	17	18.9	20.6	22.4	24.4	26.3	27.3	28.1	30.6	32.9	34.6	34.8
6	0.056	-1734.806	21.8	19.8	18.2	17.2	19.2	21.1	22.2	23.3	25.4	27.3	28.7	29.7
7	0.086	-1823.77	24.8	22.4	20.6	18.9	17.3	18.3	19.5	20.4	22.3	24.2	25.9	27.3
8	0.096	-2250.799	30.8	28.3	25.9	23.7	21.6	19.7	19.1	20.2	22.6	25	27.3	28.7
9	0.11	-2535.485	34.7	32.8	30	27.4	25	22.7	21.6	20.6	21.8	24.3	26.6	28
10	0.131	-2829.068	34.8	33.3	31.8	30.3	28.8	26.2	24.9	23.7	21.3	22.6	24.8	26.1
11	0.155	-2197.421	25.9	24.3	22.8	21.3	20	18.9	18.4	18	17.2	16.4	17.4	20.7
12	0.16	-1378.948	17.4	16.4	15.3	14.3	14.2	13.8	13.7	13.5	13.1	12.7	12.9	15.6
13	0.105	-578.2686	11.3	9.4	8	8.4	16.2	21.6	23.7	26.2	30.2		33.4	33.7
14	-0.035	-100	14.2	14.7	15	20.9	26.9	31.5	32.3	32.9	33.9		34.9	34.6
15	-0.096	-50	11	10.4	11.4	12	12.1	12.9	13.4	13.7	12.7		8.7	8.1

Table A-10. Maximum Contact Stress for Bottom STAR Polymer Component

STAR Contact Pressure for Bottom Polymer Component														
Step Number	Rotation applied (radians)	Force applied (N)	Extreme Valgus	Moderate Valgus	Slight Valgus	Normal Valgus C	Normal Valgus B	Normal Valgus A	Baseline	Normal Varus A	Normal Varus B	Slight Varus	Moderate Varus	Extreme Varus
1	-0.061	-222.411	43.3	45.3	46.7	47.4	47.7	47.8	47.8	47.7	47.5	47.1	46.5	45.8
2	-0.07	-756.1974	58.8	60.4	61.3	61.6	61.6	61.5	61.4	61.2	60.8	60.4	59.7	58.7
3	-0.03	-756.2	54.7	54.4	54.1	53.9	53.6	53.4	53.3	53.2	53	52.5	51.7	49.3
4	0	-756.1974	53	53.1	52.9	52.6	52.4	52	51.8	51.6	51	50.1	48.4	45.6
5	0.014	-1512.395	62.6	62.5	61.8	61.1	60.3	59.6	59.2	58.8	58.1	57.3	56.1	54.3
6	0.056	-1734.806	68.1	65.8	66	66.1	66	65.9	65.8	65.7	65.5	65.3	64.8	63.6
7	0.086	-1823.77	84.2	78.9	75.2	74	74.3	74.4	74.4	74.4	74.2	73.9	73.1	72
8	0.096	-2250.799	97.1	91.7	86.8	82.4	82.5	82.5	82.3	82.2	81.7	81.1	80.1	78.7
9	0.11	-2535.485	111.5	105	98.6	93	91	91.1	91	90.8	90.2	89.4	88.1	86.1
10	0.131	-2829.068	122.7	116.7	111.5	106	100.3	97.1	96.9	96.6	95.8	94.7	93.3	90.7
11	0.155	-2197.421	117.8	111.6	105.1	100.3	95.8	91.8	93.3	94.7	96.8	95.5	93.7	91.2
12	0.16	-1378.948	97.4	92.2	86.8	81.6	77.6	74.4	76	77.4	79.5	80.3	80.6	79.3
13	0.105	-578.2686	66.3	75.5	81.8	86.1	87.7	88.9	89.2	89.5	89.8		90.2	90.2
14	-0.035	-100	29.7	31.4	31.6	31.4	30.7	30.2	30	29.7	29.2		28.5	27.7
15	-0.096	-50	21.8	21.9	22.2	21.9	21.8	22.4	22.9	23.3	23.1		20.1	19.7

Table A-11. Maximum Contact Pressure for STAR Talar Component

STAR Contact Pressure for Talar Component														
Step Number	Rotation applied (radians)	Force applied (N)	Extreme Valgus	Moderate Valgus	Slight Valgus	Normal Valgus C	Normal Valgus B	Normal Valgus A	Baseline	Normal Varus A	Normal Varus B	Slight Varus	Moderate Varus	Extreme Varus
1	-0.061	-222.411	18.9	20.3	21	21.4	21.5	21.5	21.5	21.5	21.4	21.1	20.8	20.5
2	-0.07	-756.1974	35.9	31.1	31.7	31.9	31.9	31.7	31.5	31.4	31	30.5	31.3	33.6
3	-0.03	-756.2	28.3	28.3	28.2	28	27.7	27.5	27.3	27.1	26.6	26.1	25.4	23.9
4	0	-756.1974	28.8	28.9	28.8	28.6	28.4	28.1	28	27.8	27.4	26.7	25.9	24.4
5	0.014	-1512.395	38	35.8	35.5	35	34.6	34	33.7	33.4	32.8	32.2	31.4	30.2
6	0.056	-1734.806	47.4	43.2	40.3	37.9	37.6	37.2	37	36.7	36.2	35.4	34.5	33.3
7	0.086	-1823.77	52.7	47.1	43.5	40.9	40.7	40.3	40	39.7	38.8	37.7	36.4	35
8	0.096	-2250.799	61.6	57.2	52.7	48.3	44	43.4	43.1	42.8	41.8	40.7	39.1	41.2
9	0.11	-2535.485	69.2	64.6	60.4	57.6	54.5	51.3	49.6	47.9	44.5	41.7	43.9	46.5
10	0.131	-2829.068	72.5	69	65.6	62.3	59	56.4	55.2	54.1	52.1	50.4	48.9	49.5
11	0.155	-2197.421	70.4	66.2	62.2	58.4	54.8	51.5	50	48.5	45.7	43.7	42.1	43.2
12	0.16	-1378.948	61.5	56.4	51.8	47.3	43.4	39.7	38.1	36.7	39	40.1	40.8	40
13	0.105	-578.2686	28.9	32.6	34.8	36.5	37	38.3	38.8	39.1	39.4		39.9	40.1
14	-0.035	-100	17.6	17.7	17.6	17.4	17.4	17.3	17.2	17	16.7		15.8	15.1
15	-0.096	-50	10.2	9.8	8.4	8.7	9.1	9.6	9.9	10.1	10.1		8.6	8.1

REFERENCES

1. Stauffer, R.N., E.Y. Chao, and R.C. Brewster, *Force and motion analysis of the normal, diseased, and prosthetic ankle joint.* Clin Orthop Relat Res, 1977(127): p. 189-96.

2. Cracchiolo, A., 3rd and J.K. Deorio, *Design features of current total ankle replacements: implants and instrumentation.* J Am Acad Orthop Surg, 2008. 16(9): p. 530-40.

3. Valderrabano, V., et al., *Etiology of ankle osteoarthritis.* Clin Orthop Relat Res, 2009. 467(7): p. 1800-6.

4. Coester, L.M., et al., *Long-term results following ankle arthrodesis for post-traumatic arthritis.* J Bone Joint Surg Am, 2001. 83-A(2): p. 219-28.

5. Flavin, R., et al., *Comparison of gait after total ankle arthroplasty and ankle arthrodesis.* Foot Ankle Int, 2013. 34(10): p. 1340-8.

6. Frigg, A., et al., *Clinical relevance of hindfoot alignment view in total ankle replacement.* Foot Ankle Int, 2010. 31(10): p. 871-9.

7. Andrews, J.R., W.J. Previte, and W.G. Carson, *Arthroscopy of the ankle: technique and normal anatomy.* Foot Ankle, 1985. 6(1): p. 29-33.

8. Huch, K., K.E. Kuettner, and P. Dieppe, *Osteoarthritis in ankle and knee joints.* Semin Arthritis Rheum, 1997. 26(4): p. 667-74.

9. Akiyama, K., et al., *Three-dimensional distribution of articular cartilage thickness in the elderly talus and calcaneus analyzing the subchondral bone plate density.* Osteoarthritis Cartilage, 2012. 20(4): p. 296-304.

10. Wapner, K.L., *Transfibular Ankle Fusion Technique.* Techniques in Foot and Ankle Surgery, 2002. 1(1): p. 17-23.

11. Arthrex. *Ankle Fusion Plating System Surgical Technique*. 2015 [cited 2016; Available from: http://www.footsurgeryatlas.com/content/uploads/2015/12/Arthrex-Ankle-Fusion-Plate-Surgical-Technique.pdf.

12. USA, B.a.J.I. *Ankle Arthrodesis.* FootCareMD A step in the right direction 2016 [cited 2016; Available from: http://www.aofas.org/footcaremd/treatments/Pages/Ankle-Arthrodesis.aspx.

13. Haddad, S.L., et al., *Intermediate and long-term outcomes of total ankle arthroplasty and ankle arthrodesis. A systematic review of the literature.* J Bone Joint Surg Am, 2007. 89(9): p. 1899-905.

14. Hahn, M.E., et al., *Comparative gait analysis of ankle arthrodesis and arthroplasty: initial findings of a prospective study.* Foot Ankle Int, 2012. 33(4): p. 282-9.

15. Jay Elliot, B., D. Gundapaneni, and T. Goswami, *Finite element analysis of stress and wear characterization in total ankle replacements.* J Mech Behav Biomed Mater, 2014. 34: p. 134-45.

16. Small Bone Innovations, I. *STAR The Only Mobile-Bearing Total Ankle Approved in the U.S. Surgical Technique*. 2009 [cited 2016; Available from: http://www.totalsmallbone.com/pdf/STAR_Surgical_Technique.pdf.

17. Latham, W.C. and J.T. Lau, *Total Ankle Arthroplasty: An Overview of the Canadian Experience.* Foot Ankle Clin, 2016. 21(2): p. 267-81.

18. Zimmer. *Zimmer Trabecular Metal Total Ankle Surgical Technique*. 2014 [cited 2016; Available from: http://www.zimmer.com/content/dam/zimmer-web/documents/en-US/pdf/surgical-techniques/foot-and-ankle/zimmer-trabecular-metal-total-ankle-surgical-technique.pdf.

19. Goetz, J.E., et al., *Variable Volumes of Resected Bone Resulting From Different Total Ankle Arthroplasty Systems.* Foot Ankle Int, 2016. 37(8): p. 898-904.

20. Saltzman, C.L. and G.Y. el-Khoury, *The hindfoot alignment view.* Foot Ankle Int, 1995. 16(9): p. 572-6.

21. Lee, W.C., et al., *Alignment of ankle and hindfoot in early stage ankle osteoarthritis.* Foot Ankle Int, 2011. 32(7): p. 693-9.

22. Tanaka, Y., et al., *Hindfoot alignment of hallux valgus evaluated by a weightbearing subtalar x-ray view.* Foot Ankle Int, 1999. 20(10): p. 640-5.

23. Reggiani, B., et al., *Finite element analysis of a total ankle replacement during the stance phase of gait.* J Biomech, 2006. 39(8): p. 1435-43.

24. Hoagland, T.M. *Ankle Joint Anatomy: Overview, Lateral Ligament Anatomy and Biomechanics, Medial Ligament Anatomy and Biomechanics*. Medscape Reference 2015. 1-5.

25. Anderson, D.D., et al., *Intra-articular contact stress distributions at the ankle throughout stance phase-patient-specific finite element analysis as a metric of degeneration propensity.* Biomech Model Mechanobiol, 2006. 5(2-3): p. 82-9.

26. Calhoun, J.H., et al., *A comprehensive study of pressure distribution in the ankle joint with inversion and eversion.* Foot Ankle Int, 1994. 15(3): p. 125-33.